ON RIEMANN SOLUTIONS TO WEAKLY HYPERBOLIC SYSTEMS: PART 2. MODELING SUPERCRITICAL FLOWS IN ARTERIES

EE HAN*, GERALD WARNECKE †, ELEUTERIO F. TORO ‡, AND ANNUNZIATO SIVIGLIA §

Abstract. This work focuses on the construction of the solution of the Riemann problem for a 3×3 first-order system that governs blood flow in compliant vessels of medium to large size. The challenge in finding the solution is posed by the admission of discontinuous material properties of the vessels, a discontinuous tube law to close the system and the admission of supercritical Riemann initial data. The corresponding Riemann solutions with subcritical initial data have been reported in [13].

Due to the high nonlinearity of the tube law and the discontinuous variation of vessel mechanical properties, the classification of the L–M and R–M curves for the supercritical data is based on two nonlinear functions with respect to the ratio of the initial material properties and the Riemann initial data. These two nonlinear functions are derived from the existence of two basic composite wave curves. In particular, the monotonicity of the basic composite wave curve containing a supercritical stationary wave, a zero speed shock and a subcritical stationary wave, is satisfied under an additional mathematical assumption. The bifurcation, which appears in certain cases of the L–M and R–M curves, leads to multiple solutions of the Riemann problem. Our results reveal the transition of blood flow from the supercritical to the subcritical state in abrupt variations of the geometrical and mechanical properties of the vessels. In the future, it would be desirable to identify physiological conditions that would help to define physically relevant solutions of the Riemann problem posed and solved here.

Key words. Physiological flows, Riemann problem, supercritical speed index, shocks, rarefactions, resonant waves, L–M curve, R–M curve

AMS subject classifications. 76Z05, 35L03, 35L60

1. Introduction. Blood flow in the cardiovascular system is very complex and is characterized by unsteady flows in deformable, even collapsible, tubes. The one dimensional formulation, or reduced models, has been extensively applied to simulate the variation of the blood vessel cross sectional area as well as the averaged blood velocity and pressure, as functions of time and the axial direction. The cross sectional averaged blood pressure is related to a tube law used as closure condition, which is given by a nonlinear pressure–area relation, involving the mechanical properties of the blood vessels. Milestone contributions on this topic can be found in, for example, [17], [29], [30], [10], [28], and references therein.

The aim of the present work is to solve the Riemann problem for the one dimensional 3×3 blood flow model proposed by Toro and Siviglia in [34] for the case of supercritical initial data. The exact Riemann solution to the resonant hyperbolic system is a weak solution as studied in [8, 14]. A considerable number of papers have been devoted to the subject of the Riemann problem for various resonant hyperbolic systems; see [26, 16, 27, 15, 20, 2, 3, 21, 32, 22, 12, 11] and the references therein. The specific challenge of the current system originates from the discontinuity of the

*Institute for Analysis and Numeric, Otto-von-Guericke-University Magdeburg, Germany (eehan84@yahoo.com).

†Institute for Analysis and Numeric, Otto-von-Guericke-University Magdeburg, Germany (gerald.warnecke@ovgu.de).

‡Laboratory of Applied Mathematics, Faculty of Engineering, University of Trento, Italy(toro@ing.unitn.it).

§Laboratory of Hydraulics, Hydrology and Glaciology (VAW), ETH Zurich, Switzerland (siviglia@vaw.baug.ethz.ch).

mechanical properties of vessels and the nonlinear tube law assumed. This paper is a continuation of the work reported in [13] for the case of subcritical data.

Most physiological flows in blood vessels are said to be characterized by subcritical conditions, see Caro et al. [5]. However, flow transition from subcritical to supercritical conditions can be generated by the presence of geometrical discontinuities as well as by mechanical property variations, see Ku [18, 19] and Siviglia Toffolon [31].

According to the framework proposed in [13], the L–M and R–M curves are introduced to handle the resonance of the hyperbolic system considered. These two curves represent the set of intermediate states associated to the left and right Riemann initial data. Moreover the classification and monotonicity of the L–M and R–M curves have been attributed to the two basic composite wave curves.

Due to the nonlinearity of the tube law and the discontinuous mechanical properties, two nonlinear functions of the ratio of the initial material properties and the Riemann initial data are derived. The L–M and R–M curves can be classified into three different cases for the case of supercritical Riemann data. They are denoted as Case III, IV and V, to keep consistency with the classification of the subcritical data case introduced in [13]. In addition, the monotonicity of the basic composite wave curve containing a supercritical stationary wave, a zero speed shock, and a subcritical stationary wave is satisfied under an extra assumption. It claims that a formula does not change sign when the variable of mechanical properties of vessels varies in its region. This formula depends on the velocity, the ratio of cross sectional areas related to a zero speed shock, as well as the density and the variable of mechanical properties of vessels. We point out that the cross sectional areas and the velocity are taken as a function of the variable of mechanical properties of vessels. The assumption has been demonstrated by examples studied in Sections 3.4 and 3.5.

Concerning the supercritical data, the L–M and R–M curves contain a bifurcation for Case IV as well as Case III, but under a certain condition. The bifurcation leads to three possible solutions for a given initial data. For the remaining cases of L–M and R–M curves, they are continuous, monotone decreasing and increasing, respectively, in the state plane. Therefore, the Riemann solution is unique in these cases. We have carefully studied and analyzed the various cases. Several examples are used to illustrate the corresponding wave configurations. We can clearly observe the transition of the blood flow from the supercritical to the subcritical state, with abrupt variations of the vessel properties. To single out the physical relevant solutions among all possible Riemann solutions, it would be desirable to identify appropriate physiological conditions, in the future.

This paper is organized as follows. In Section 2 we review the governing system and its mathematical properties. In Section 3 we study the L–M and R–M curves for the supercritical data. The behaviour of the two basic composite wave curves are fully analyzed. The cases of the L–M curves are studied in detail. Conclusions are drawn in Section 4.

2. Model and mathematical properties. The one dimensional mathematical model valid for blood flow in compliant vessels derived from the axisymmetric Navier–Stokes equations by the averaging procedure, see [34, 4, 28], is given by

$$\begin{aligned} &\partial_t A + \partial_x(Au) = 0, \\ &\partial_t(uA) + \partial_x(Au^2 + \tfrac{A\Psi}{\rho}) - \tfrac{\Psi}{\rho}\partial_x A = 0, \\ &\partial_t K = 0, \end{aligned} \tag{2.1}$$

where $A(x,t)$ is the cross sectional area of the blood vessel, $u(x,t)$ is the averaged velocity of blood flow for the cross sectional area, ρ is the constant blood density. The following tube law with respect to pressure–area relation is used to close the system (2.1):

$$\Psi(A;K) = K(x)\left[\left(\frac{A(x)}{A_0(x)}\right)^m - 1\right], \tag{2.2}$$

where $A_0(x)$ is the equilibrium cross sectional area and m is a constant parameter satisfying $0 < m < 1$. In particular the value $m = \frac{1}{2}$ correctly describes the wave propagation patterns in arterial networks, as was extensively confirmed by [1, 24]. Here the material properties of the blood vessel $K(x)$ is defined by

$$K(x) = \frac{\sqrt{\pi}}{(1-\nu^2)}\frac{E(x)h_0(x)}{\sqrt{A_0(x)}}, \tag{2.3}$$

where $h_0(x)$ is the thickness of the vessel walls, $E(x)$ is the *Young's modulus* of elasticity, and ν is the Poisson ratio. Following Ku [18], the local elastic tube pressure wave speed of (2.1) is defined as

$$c(A,K) = \sqrt{\frac{mK}{\rho}\left(\frac{A}{A_0}\right)^m}. \tag{2.4}$$

It is analogous to the sound speed in gas dynamics, see [12].

The Riemann initial data for the system (2.1) are two constant states separated by a discontinuity and given as follows

$$(K,A,u)(x,0) = \begin{cases} (K_L,\ A_L,\ u_L), & x < 0, \\ (K_R,\ A_R,\ u_R), & x > 0. \end{cases} \tag{2.5}$$

Without loss of generality, in this work we always assume that

$$K_L > K_R. \tag{2.6}$$

The opposite Riemann problem can be treated as a mirror–image problem by setting the velocity in the inverse direction. Note that the pressure wave speed $c(A,K)$ in (2.4) depends on K. This leads to a discontinuity of the wave speed in the state plane. For the sake of clarity, we let $c_L = c(A_L,K_L)$ and $c_R = (A_R,K_R)$ denote, respectively, the local elastic tube pressure wave speed of the left and right Riemann initial data. Moreover the speed index of the current system is

$$S^I = \frac{u}{c}. \tag{2.7}$$

It is analogous to the Mach number for gas dynamics and the Froude number in free surface fluid dynamics, i.e. if $|S^I| < 1$, the blood flow is subcritical; if $|S^I| > 1$ the blood flow is supercritical; otherwise, the blood flow is critical.

The system (2.1) is weakly or resonant hyperbolic. It has three characteristic fields with the eigenvalues $\lambda_1 = u - c$, $\lambda_2 = u$, and $\lambda_3 = u + c$. Three different elementary waves are associated to the corresponding characteristic fields. We use the terminology j–wave, $j = 0, 1, 2$, to denote the corresponding waves when the eigenvalues are distinct from each other. Specifically the 1– and 2–waves are shocks

or rarefactions. The 0–wave is a stationary wave located at $x = 0$ due to the jump of the variable K at $x = 0$.

One knows that the Riemann solution to a hyperbolic system is self–similar. In addition the system (2.1) degenerates at the critical states $u = \pm c$, i.e. $S^I = 1$. Due to it, the 1– or 2–waves might coincide with the stationary wave. That is to say the waves of different families will be combined together. The resonant waves are defined to take into account of these combined waves. Generally there are two types of the wave configurations to the Riemann solutions. One type is without the resonant waves and the other type is with the resonant waves. The wave configuration with the resonant waves consist of a resonant wave and a 1– or 2–wave. While the wave configurations without the resonant waves are classical. They consist of four constant regions separated by three elementary waves.

We now denote $\mathbf{w} = (A, u)^T$ and briefly recall the elementary wave curves. The detailed derivation can be found in [13, 34]. The nonlinear 1– and 2–waves consist of shocks and rarefactions. The corresponding wave curves denoted as $T_1(\mathbf{w}_L)$ and $T_2(\mathbf{w}_R)$, respectively, can be described entirely as a one parameter family of states given by

$$T_1(\mathbf{w}_q) = \{\mathbf{w} | u = u_L - f(A; \mathbf{w}_L),\ A > 0\}, \tag{2.8}$$

$$T_2(\mathbf{w}_q) = \{\mathbf{w} | u = u_R + f(A; \mathbf{w}_R),\ A > 0\}, \tag{2.9}$$

where

$$f(A; \mathbf{w}_q) := \begin{cases} \frac{2}{m}\left(\sqrt{\frac{mK_q}{\rho}\left(\frac{A}{A_0}\right)^m} - c_q\right), & \text{if } A \le A_q, \\ \frac{c_q}{\sqrt{m+1}}\left[\left(\left(\frac{A}{A_q}\right)^{m+1} - 1\right)\left(1 - \frac{A_q}{A}\right)\right]^{\frac{1}{2}}, & \text{if } A > A_q. \end{cases} \tag{2.10}$$

Note that the states with $A \le A_q$ are related to the rarefaction curves, while the states with $A > A_q$ are related to the shock wave curves.

The 0–wave is a stationary wave. Two states $\mathbf{w}_{in}$ and $\mathbf{w}_{out}$ connected by the stationary wave satisfy the relations

$$A_{out} u_{out} = A_{in} u_{in}, \tag{2.11}$$

$$\frac{1}{2}\rho u_{out}^2 + K_{out}\left[\left(\frac{A_{out}}{A_0}\right)^m - 1\right] = \frac{1}{2}\rho u_{in}^2 + K_{in}\left[\left(\frac{A_{in}}{A_0}\right)^m - 1\right]. \tag{2.12}$$

For simplicity we can use the notation $\mathbf{w}_{out} = \mathbf{J}(K_{out}; \mathbf{w}_{in}, K_{in})$ to represent the explicit solution $\mathbf{w}_{out}$ implicitly given by (2.11) and (2.12), where

$$\begin{cases} K_{in} = K_L, \\ K_{out} = K_R, \end{cases} \quad \text{when } u_{in} > 0, \quad \text{and} \quad \begin{cases} K_{in} = K_R, \\ K_{out} = K_L, \end{cases} \quad \text{when } u_{in} < 0. \tag{2.13}$$

Here we take the discontinuous K as the limiting case of piecewise monotonic mechanical property variables with slope going to infinity. The stationary wave is viewed as a transition layer located at $x = 0$ with 0 width. The wave curve for the stationary wave cannot be expressed explicitly like $T_1(\mathbf{w}_L)$ and $T_2(\mathbf{w}_R)$. As we have introduced in [13], the velocity of the outflow state for the stationary wave curve is determined by the root of the following velocity function

$$\phi(u; \mathbf{w}_{in}, K_{in}, K_{out}) := \frac{1}{2}\rho u^2 + K_{out}\left[\left(\frac{A_{in}u_{in}}{A_0 u}\right)^m - 1\right] - \frac{1}{2}\rho u_{in}^2 - K_{in}\left[\left(\frac{A_{in}}{A_0}\right)^m - 1\right]. \tag{2.14}$$

The solution to $\phi(u; \mathbf{w}_{in}, K_{in}, K_{out}) = 0$ can be found in [13, p. 8, Corollary 2.3].

3. L–M and R–M curves for the supercritical state. The challenge for solving the Riemann problem is twofold. The first is how to determine the mutual position of the stationary wave and the remaining elementary waves a priori. The second is how to uniformly calculate all possible Riemann solutions in case that the 1–wave or 2–wave coincide with the stationary wave. In such kind of case, resonant waves are introduced. The resolution is to define the L–M and R–M curves. They are the combination of the stationary wave curve with the 1–wave curve and the 2–wave curve respectively. The present work will focus on the L–M and R–M curves for supercritical states. The classification and properties of L–M and R–M curves have been attributed to two basic composite wave curves, see [13, Sec. 3].

The first basic composite wave curve denoted as $P^j_{ES}(\mathbf{w}_q)$, $j = 1, 2$, is the combination of a j–wave and a stationary wave. The second basic composite wave curve denoted as $P^j_{s0s}(\mathbf{w}_q)$ is resonant due to the coincidence of the stationary wave with a zero speed shock. This zero speed shock splits the stationary wave into two parts. One part is a supercritical stationary wave. The other part is a subcritical stationary wave. Before investigating the two composite wave curves with the supercritical state $\mathbf{w}_q$, we need to consider two critical values

$$u^L_{col} = u_L + \frac{2}{m}c_L, \qquad u^R_{col} = u_R - \frac{2}{m}c_R. \tag{3.1}$$

They are used to indicate the collapsible state of vessels and satisfy $u^L_{col} > 0$ if $u_L > c_L$, and $u^R_{col} < 0$ if $u_R + c_R < 0$. This implies that the L–M and R–M curves in the (u, A) state plane meet the critical line $A = 0$ before the stationary wave is attached to them. Consequently, the Riemann solution that has the wave configuration A^1_{col}, see [13, Figure 3.13], cannot exist for the supercritical state.

3.1. The supercritical basic wave curve $P^j_{ES}(\mathbf{w}_q)$. It is defined as

$$P^j_{ES}(\mathbf{w}_q) = \{\mathbf{w} | \mathbf{w} = J(K_{out}; \mathbf{w}_-, K_{in}), \mathbf{w}_- \in T_j(\mathbf{w}_q); S_q(A_-; \mathbf{w}_q) \gtrless 0, u_- \lesseqgtr 0\}, \tag{3.2}$$

where K_{in} and K_{out} are in (2.13) and $S_j(A_-; \mathbf{w}_q)$ represents the j–wave speed, for $j = 1, 2$, given by

$$S_j(A_-; \mathbf{w}_q) = \begin{cases} u_- \pm c_-, & A_- \le A_q, \\ \sigma_j(A_-; \mathbf{w}_q), & A_- > A_q. \end{cases}$$

To satisfy the restriction $S_1(A_-; \mathbf{w}_L) < 0$ and $u_- > 0$, the minimum blood vessel area $A^{P^1_{ES}}_{min}$ and the maximum blood vessel area $A^{P^1_{ES}}_{max}$ are introduced. Due to $u_L > c_L$, we have

$$A^{P^l_{ES}}_{min} = \hat{A}_{1,L}, \quad A^{P^l_{ES}}_{max} = A_{u^0_1}. \tag{3.3}$$

Analogously, for $P^2_{ES}(\mathbf{w}_R)$, we have

$$A^{P^2_{ES}}_{min} = \hat{A}_{2,R}, \quad A^{P^2_{ES}}_{max} = A_{u^0_2}. \tag{3.4}$$

The cross sectional areas $A_{u^0_j}$, $j = 1, 2$, are defined in [13, (3.17)]. Moreover the terminology $\hat{\mathbf{w}}_{j,q}$ is used to denote the state that can be connected to $\mathbf{w}_q$ by a zero speed j–shock, $j = 1, 2$. The components of $\hat{\mathbf{w}}_{j,q}$ can be calculated from

$$\hat{A}_{j,q} = A_q x_{s^0_j}, \quad \hat{u}_{j,q} = \frac{A_q u_q}{\hat{A}_{j,q}}, \tag{3.5}$$

where $x_{s_j^0}$ is the solution to the following equation

$$x^{m+2} - \left[1 + (m+1)\left(\frac{u_q}{c_q}\right)^2\right] x + (m+1)\left(\frac{u_q}{c_q}\right)^2 = 0. \tag{3.6}$$

The details of this part can be found in [13, p. 5-6].

For the existence of $P_{ES}^j(\mathbf{w}_q)$ we have attributed it to $\Omega_q(A; \mathbf{w}_q, K_{in}, K_{out}) \leq 0$, where

$$\begin{aligned}\Omega_q(A; \mathbf{w}_q, K_{in}, K_{out}) \quad := \quad & \tfrac{m+2}{2}\left(\tfrac{\rho}{m}\right)^{\frac{m}{m+2}} K_{out}^{\frac{2}{m+2}} \left(\tfrac{AU(A;\mathbf{w}_q)}{A_0}\right)^{\frac{2m}{m+2}} - \tfrac{\rho U(A;\mathbf{w}_q)^2}{2} \\ & -K_{in}\left(\tfrac{A}{A_0}\right)^m + K_{in} - K_{out},\end{aligned} \tag{3.7}$$

and $U(A; \mathbf{w}_q) := u_q \pm f(A; \mathbf{w}_q)$. The derivation details can be found in [13, Sec. 3.1.2].

LEMMA 3.1. *The function $\Omega_q(A; \mathbf{w}_q, K_{in}, K_{out})$ is decreasing if $A_{min}^{P_{ES}^l} < A < A_{max}^{P_{ES}^l}$ and $u_q^2 > c_q^2$.*

Proof. It is necessary to prove that $\Omega_q'(A; \mathbf{w}_q, K_{in}, K_{out}) < 0$. We just focus on $\Omega_l'(A; \mathbf{w}_L, K_L, K_R) < 0$. The case $\Omega_r'(A; \mathbf{w}_R, K_R, K_L) < 0$ can be treated likewise. Note that

$$\Omega_l'(A; \mathbf{w}_L, K_L, K_R) \quad = \quad \tfrac{\rho}{A}\left(\tfrac{K_R}{K_L}\right)^{\frac{2}{m+2}} c(A)^{\frac{4}{m+2}} U(A; \mathbf{w}_L)^{\frac{m-2}{m+2}} w(A) + \tfrac{\rho}{A}\mu(A), \tag{3.8}$$

where

$$w(A) := U(A; \mathbf{w}_L) - Af'(A; \mathbf{w}_L) \tag{3.9}$$

and

$$\mu(A) := AU(A; \mathbf{w}_L) f'(A; \mathbf{w}_L) - c(A)^2. \tag{3.10}$$

Since $A > 0$, $\rho > 0$, $c(A) > 0$, and $U(A; \mathbf{w}_L) > 0$, we turn to prove that $w(A) < 0$ and $\mu(A) < 0$. Due to $A_L < \hat{A}_{1,L} < A < A_{u_1^0}$ and (2.10), we obtain that

$$\begin{aligned} w'(A) \quad = \quad & -\frac{c_L}{4A_L\sqrt{(m+1)\left[\left(\frac{A}{A_L}\right)^{m+1} - \left(\frac{A}{A_L}\right)^m + \frac{A_q}{A} - 1\right]}} \left\{4\left[(m+1)\left(\tfrac{A}{A_L}\right)^m - m\left(\tfrac{A}{A_L}\right)^{m-1}\right.\right. \\ & \left.\left. - \left(\tfrac{A}{A_L}\right)^{-2}\right]\left[\left(\tfrac{A}{A_L}\right)^{m+1} - \left(\tfrac{A}{A_L}\right)^m + \tfrac{A_L}{A} - 1\right] + \tfrac{A}{A_L} g(A)\right\}, \end{aligned} \tag{3.11}$$

where

$$\begin{aligned} g(A) = 2\left[m(m+1)\left(\frac{A}{A_q}\right)^{m-1} - m(m-1)\left(\frac{A}{A_q}\right)^{m-2} + 2\left(\frac{A}{A_q}\right)^{-3}\right]\left[\left(\frac{A}{A_q}\right)^{m+1} - \right. \\ \left. \left(\frac{A}{A_q}\right)^m + \left(\frac{A}{A_q}\right)^{-1} - 1\right] - \left[(m+1)\left(\frac{A}{A_q}\right)^m - m\left(\frac{A}{A_q}\right)^{m-1} - \left(\frac{A}{A_q}\right)^{-2}\right]^2. \end{aligned}$$

After a lengthy calculation, (3.11) can be simplified to

$$\begin{aligned} w'(A) \quad = \quad & \beta\left[(m+1)(m+3)\left(\tfrac{A}{A_L}\right)^{2m+1} - 2(m+1)(m+2)\left(\tfrac{A}{A_L}\right)^{2m} + m(m+2)\right. \\ & \left(\tfrac{A}{A_L}\right)^{2m-1} - 2(m+1)(m+2)\left(\tfrac{A}{A_L}\right)^m + 2(2m^2+5m+3)\left(\tfrac{A}{A_L}\right)^{m-1} \\ & \left. -2m(m+2)\left(\tfrac{A}{A_L}\right)^{m-2} - \left(\tfrac{A}{A_L}\right)^{-3}\right] < 0, \end{aligned} \tag{3.12}$$

where $\beta = -\frac{c_L}{4A_L\sqrt{m+1}}\left\{\left(\frac{A}{A_L}\right)^{m+1} - \left(\frac{A}{A_L}\right)^{m} + \frac{A_L}{A} - 1\right\}^{-\frac{1}{2}}$. This implies that the function $w(A)$ is decreasing.

Due to $A_{min}^{P_{ES}^l} < A < A_{max}^{P_{ES}^l}$ and (3.3), for (3.9) we only need to prove the following fact

$$w(\hat{A}_{1,L}) = \hat{u}_{1,L} - \hat{A}_{1,L} f'(\hat{A}_{1,L}; \mathbf{w}_L) < 0. \tag{3.13}$$

The left part of the inequality (3.13) equals to

$$w(\hat{A}_{1,L}) = \frac{A_L u_L}{\hat{A}_{1,L}} - \hat{A}_{1,L}\frac{c_L}{2A_L\sqrt{m+1}}\frac{(m+1)\left(\frac{\hat{A}_{1,L}}{A_L}\right)^m - m\left(\frac{\hat{A}_{1,L}}{A_L}\right)^{m-1} - \left(\frac{A_L}{\hat{A}_{1,L}}\right)^2}{\sqrt{\left(\left(\frac{\hat{A}_{1,L}}{A_L}\right)^{m+1} - 1\right)\left(1 - \frac{A_L}{\hat{A}_{1,L}}\right)}}. \tag{3.14}$$

We denote $\hat{x} = \frac{\hat{A}_{1,L}}{A_L} > 1$. The formula (3.14) can be rewritten as

$$\begin{aligned} w(\hat{A}_{1,L}) &= \frac{u_L}{\hat{x}} - \frac{c_L\hat{x}}{2\sqrt{m+1}}\frac{(m+1)\hat{x}^m - m\hat{x}^{m-1} - \hat{x}^{-2}}{\sqrt{(\hat{x}^{m+1}-1)(1-\hat{x}^{-1})}} \\ &= \frac{c_L}{\hat{x}\sqrt{m+1}}\left[\sqrt{m+1}\frac{u_L}{c_L} - \frac{1}{2}\frac{(m+1)\hat{x}^{m+2} - m\hat{x}^{m+1} - 1}{\sqrt{(\hat{x}^{m+1}-1)(1-\hat{x}^{-1})}}\right]. \end{aligned} \tag{3.15}$$

Note that $\hat{A}_{1,L}$ and A_L are connected by a 0–speed shock. The equation (3.6) yields

$$\sqrt{m+1}\frac{u_L}{c_L} = \sqrt{\frac{\hat{x}(\hat{x}^{m+1}-1)}{\hat{x}-1}}. \tag{3.16}$$

Inserting (3.16) into (3.15) and under the condition $\hat{x} > 1$, we obtain that

$$w(\hat{A}_{1,L}) = \frac{c_L}{2\sqrt{m+1}\sqrt{\hat{x}\,(\hat{x}^{m+1}-1)(1-\hat{x})}}\left[-(m+1)\hat{x}^{m+2} + (m+2)\hat{x}^{m+1} - 1\right] < 0. \tag{3.17}$$

Next we turn to prove (3.10). Note that

$$\mu'(A) = w'(A)f'(A;\mathbf{w}_L) + AU(A;\mathbf{w}_L)f''(A;\mathbf{w}_L) - \frac{mc(A)^2}{A}. \tag{3.18}$$

From [13, (2.18), (2.19)], we get $f'(A;\mathbf{w}_L) > 0$ and $f''(A;\mathbf{w}_L) < 0$. Since (3.12), we have $\mu'(A) < 0$. Next we turn to determine the sign of $\mu(\hat{A}_{1,L})$. Due to the relations for the zero speed shock, $c(\hat{A}_{1,L})^2 = c_L^2\left(\frac{\hat{A}_{1,L}}{A_L}\right)^m = c_L^2\hat{x}^m$ is satisfied and we have $\hat{A}_{1,L}\hat{u}_{1,L} = A_L u_L$. Thus we obtain

$$\begin{aligned} \mu(\hat{A}_{1,L}) &= \frac{u_L c_L}{2\sqrt{m+1}}\frac{(m+1)\hat{x}^m - m\hat{x}^{m-1} - \hat{x}^{-2}}{\sqrt{(\hat{x}^{m+1}-1)(1-\hat{x}^{-1})}} - c_L^2\hat{x}^m \\ &= \frac{c_L^2}{2(m+1)}\left[\sqrt{m+1}\frac{u_L}{c_L}\frac{(m+1)\hat{x}^m - m\hat{x}^{m-1} - \hat{x}^{-2}}{\sqrt{(\hat{x}^{m+1}-1)(1-\hat{x}^{-1})}} - 2(m+1)\hat{x}^m\right] \end{aligned} \tag{3.19}$$

Inserting (3.16) into (3.19) and simplifying the formula, with $\hat{x} > 1$ leads to

$$\mu(\hat{A}_{1,L}) = \frac{c_L^2}{2(m+1)\hat{x}(\hat{x}-1)}\left(-(m+1)\hat{x}^{m+2} + (m+2)\hat{x}^{m+1} - 1\right) < 0. \tag{3.20}$$

This completes the proof of the lemma. □

Inserting $(\hat{A}_{1,L}, \hat{u}_{1,L})$ into (3.7) we obtain

$$\Omega_l(\hat{A}_{1,L}; \mathbf{w}_L, K_L, K_R) = \frac{m+2}{2m}\rho\left(\frac{K_R}{K_L}\hat{u}_{1,L}^m \hat{c}_{1,L}^2\right)^{\frac{2}{m+2}} - \frac{1}{2}\rho\hat{u}_{1,L}^2 - \frac{\rho}{m}\hat{c}_{1,L}^2 + K_L - K_R. \tag{3.21}$$

Since $\hat{u}_{1,L} = \frac{A_L u_L}{\hat{A}_{1,L}}$ and $\hat{c}_{1,L} = c_L\left(\frac{\hat{A}_{1,L}}{A_L}\right)^{\frac{m}{2}}$, the equation (3.21) can be rewritten as

$$\begin{aligned}\Omega_l(\hat{A}_{1,L}; \mathbf{w}_L, K_L, K_R) &= \tfrac{m+2}{2m}\rho\left(\tfrac{K_R}{K_L}u_L^m c_L^2\right)^{\frac{2}{m+2}} - \tfrac{1}{2}\rho u_L^2\left(\tfrac{\hat{A}_{1,L}}{A_L}\right)^{-2} \\ &\quad - \tfrac{\rho}{m}c_L^2\left(\tfrac{\hat{A}_{1,L}}{A_L}\right)^m + K_L - K_R.\end{aligned} \tag{3.22}$$

Multiplying (3.22) by $\frac{m}{\rho c_L^2}$, we obtain that

$$\begin{aligned}\frac{m}{\rho c_L^2}\Omega_l(\hat{A}_{1,L}; \mathbf{w}_L, K_L, K_R) &= \frac{m+2}{2}\left(\frac{K_R}{K_L}\right)^{\frac{2}{m+2}}\left(\frac{u_L}{c_L}\right)^{\frac{2m}{m+2}} - \frac{m}{2}\left(\frac{u_L}{c_L}\right)^2\left(\frac{\hat{A}_{1,L}}{A_L}\right)^{-2} \\ &\quad - \left(\frac{\hat{A}_{1,L}}{A_L}\right)^m + \left(1 - \frac{K_R}{K_L}\right)\left(\frac{A_L}{A_0}\right)^{-m}.\end{aligned} \tag{3.23}$$

We define $\kappa = \frac{K}{K_L}$. The relation (3.23) suggests to introduce the following function with respect to κ

$$\begin{aligned}\varphi(\kappa; \mathbf{w}_L) &= \tfrac{m+2}{2}\left(\tfrac{u_L}{c_L}\right)^{\frac{2m}{m+2}}\kappa^{\frac{2}{m+2}} - \left(\tfrac{A_0}{A_L}\right)^m\kappa - \tfrac{m}{2}\left(\tfrac{u_L}{c_L}\right)^2\left(\tfrac{\hat{A}_{1,L}}{A_L}\right)^{-2} \\ &\quad - \left(\tfrac{\hat{A}_{1,L}}{A_L}\right)^m + \left(\tfrac{A_L}{A_0}\right)^{-m}.\end{aligned} \tag{3.24}$$

The existence of $P_{ES}^1(\mathbf{w}_L)$ is summarized in the following lemma.

LEMMA 3.2. *Assume that $u_L > c_L$ and $A_{max}^{P_{ES}^l} \geq A_0\left[1 - \frac{K_R}{K_L}\right]^{\frac{1}{m}}$, we have:*

1. *If $\varphi\left(\frac{K_R}{K_L}; \mathbf{w}_L\right) \leq 0$ then the composite wave $P_{ES}^1(\mathbf{w}_L)$ always exists;*
2. *Otherwise if $\varphi\left(\frac{K_R}{K_L}; \mathbf{w}_L\right) > 0$, the existence region for $P_{ES}^1(\mathbf{w}_L)$ is $\tilde{A}_{l,sup}^c < A_- < A_{max}^{P_{ES}^1}$, where $\tilde{A}_{l,sup}^c$ is the solution to $\Omega_l(A; \mathbf{w}_L, K_L, K_R) = 0$.*

In the same manner, we summarize the results for the existence of the basic composite wave curve $P_{ES}^2(\mathbf{w}_R)$ in the following lemma.

LEMMA 3.3. *Assume that $u_R + c_R < 0$, we have:*

1. *If $\varphi\left(\frac{K_L}{K_R}; \mathbf{w}_R\right) \leq 0$ then $P_{ES}^2(\mathbf{w}_R)$ always exists;*
2. *Otherwise if $\varphi\left(\frac{K_L}{K_R}; \mathbf{w}_R\right) > 0$, the existence region for $P_{ES}^2(\mathbf{w}_R)$ is $\tilde{A}_{r,sup}^c < A_- < A_{max}^{P_2^r}$, where $\tilde{A}_{r,sup}^c$ is the solution to $\Omega_r(A; \mathbf{w}_R, K_R, K_L) = 0$.*

REMARK 3.4. *We denote*

$$\tilde{u}_{q,sup}^c = u_q \pm f(\tilde{A}_{q,sup}^c; \mathbf{w}_q). \tag{3.25}$$

Due to the fact that $\Omega_q\left(\tilde{A}_{q,sup}^c; \mathbf{w}_q, K_{in}, K_{out}\right) = 0$ the outflow state $\mathbf{w}^c = J(K_{out}; \tilde{\mathbf{w}}_{q,sup}^c, K_{in})$ is critical.

REMARK 3.5. *The monotonicity of $P_{ES}^j(\mathbf{w}_q)$ has been entirely determined in [13, p. 15, Lemma 3.8]. Specifically the curve $P_{ES}^1(\mathbf{w}_L)$ is continuously decreasing in (u, Ψ) state plane, while the curve $P_{ES}^2(\mathbf{w}_R)$ is continuously increasing in (u, Ψ) state plane.*

3.2. The basic composite wave curve $P^j_{s0s}(\mathbf{w}_q)$. For the supercritical state $\mathbf{w}_q$, we define

$$P^j_{s0s}(\mathbf{w}_q) = \left\{\mathbf{w}|\mathbf{w} = \mathbf{J}(K_{out};\mathbf{w}_+,K); \mathbf{w}_+ = S^0_j(\mathbf{w}_-);\ \mathbf{w}_- = \mathbf{J}(K;\mathbf{w}_q,K_{in})\right\}, \tag{3.26}$$

where $K \in]K_{in}, K_{out}[$, K_{in} and K_{out} were defined in (2.13) and $j = 1, 2$. We need to consider the existence of the states $\mathbf{w}_- = J(K;\mathbf{w}_q,K_{in})$ and $\mathbf{w} = J(K_{out};\mathbf{w}_+,K)$. The existence of $\mathbf{w}_- = J(K;\mathbf{w}_q,K_{in})$ is equivalent to the relation

$$\frac{m+2}{2m}\rho\left(\frac{K}{K_{in}}u_q^m c_q^2\right)^{\frac{2}{m+2}} - \frac{1}{2}\rho u_q^2 - \frac{\rho}{m}c_q^2 + K_{in} - K \le 0. \tag{3.27}$$

Dividing by $\frac{\rho c_q^2}{m}$ and setting $\kappa = \frac{K}{K_{in}}$, we introduce a function with respect to κ given by

$$\tau(\kappa;\mathbf{w}_q) = \frac{m+2}{2}\left(\frac{u_q}{c_q}\right)^{\frac{2m}{m+2}}\kappa^{\frac{2}{m+2}} - \left(\frac{A_0}{A_q}\right)^m\kappa - \frac{m}{2}\left(\frac{u_q}{c_q}\right)^2 - 1 + \left(\frac{A_0}{A_q}\right)^m. \tag{3.28}$$

LEMMA 3.6. *For any $\mathbf{w}_q$ with $u_q^2 > c_q^2$, we have*

$$\varphi(\kappa;\mathbf{w}_q) > \tau(\kappa;\mathbf{w}_q). \tag{3.29}$$

Proof. Note that

$$\varphi(\kappa;\mathbf{w}_q) - \tau(\kappa;\mathbf{w}_q) = \frac{m}{2}\left(\frac{u_q}{c_q}\right)^2\left[1 - \left(\frac{A_q}{\hat{A}_{j,q}}\right)^2\right] - \left(\frac{\hat{A}_{j,q}}{A_q}\right)^m + 1. \tag{3.30}$$

From (3.6), we have

$$\left(\frac{u_q}{c_q}\right)^2 = \frac{1}{m+1}\frac{\left(\frac{\hat{A}_{j,q}}{A_q}\right)^{m+2} - \left(\frac{\hat{A}_{j,q}}{A_q}\right)}{\left(\frac{\hat{A}_{j,q}}{A_q}\right) - 1}. \tag{3.31}$$

Inserting (3.31) into (3.30), we obtain

$$\varphi(\kappa;\mathbf{w}_q) - \tau(\kappa;\mathbf{w}_q) = \frac{m\left(\frac{\hat{A}_{j,q}}{A_q}\right)^{m+2} - (m+2)\left(\frac{\hat{A}_{j,q}}{A_q}\right)^{m+1} + (m+2)\left(\frac{\hat{A}_{j,q}}{A_q}\right) - m}{2(m+1)\left(\frac{\hat{A}_{j,q}}{A_q}\right)} > 0, \tag{3.32}$$

since $\frac{\hat{A}_{j,q}}{A_q} > 1$. So $\varphi(\kappa;\mathbf{w}_q) > \tau(\kappa;\mathbf{w}_q)$. □

REMARK 3.7. *Lemma 3.6 tells us that if the state $\mathbf{w} = J(K_{out};\hat{\mathbf{w}}_{j,q},K_{in})$ exists, then the state $\mathbf{w} = J(K_{out};\mathbf{w}_q,K_{in})$ also exists. But the opposite relation is not true.*

Analogously we can transform the existence of the stationary wave $\mathbf{w} = \mathbf{J}(K_{out};\mathbf{w}_+,K)$ into finding a region at which $\chi(\kappa;\mathbf{w}_q) \le 0$, where

$$\begin{aligned}\chi(\kappa;\mathbf{w}_q) \quad := \quad & \tfrac{m+2}{2}\left(\tfrac{K_{out}}{\kappa K_{in}}\right)^{\frac{2}{m+2}}\left(\tfrac{u_+}{c_+}\right)^{\frac{2m}{m+2}} + \left(1 - \tfrac{K_{out}}{\kappa K_{in}}\right)\left(\tfrac{A_+}{A_0}\right)^{-m} \\ & -\tfrac{m}{2}\left(\tfrac{u_+}{c_+}\right)^2 - 1.\end{aligned} \tag{3.33}$$

Moreover the behavior of $\chi(\kappa;\mathbf{w}_q)$ is summarized in the following lemma.

LEMMA 3.8. *If* $\left(\frac{u_q}{c_q}\right)^{\frac{2m}{m+2}}\left(\frac{A_q}{A_0}\right)^m\left(\frac{K_{in}}{K_{out}}\right)^{\frac{m}{m+2}}>1$, *then* $\chi'(\kappa;\mathbf{w}_q)<0$*; Otherwise if* $\left(\frac{u_q}{c_q}\right)^{\frac{2m}{m+2}}\left(\frac{A_q}{A_0}\right)^m\left(\frac{K_{in}}{K_{out}}\right)^{\frac{m}{m+2}}<1$, *then* $\chi'(\kappa;\mathbf{w}_q)>0$.

Proof. From the definition of $P^j_{s0s}(\mathbf{w}_q)$, we have

$$c_+^2=c_q^2\left(\frac{K}{K_{in}}\right)^{\frac{2}{m+2}}\left(\frac{u_q}{c_q}\frac{c_+}{u_+}\right)^{\frac{2m}{m+2}}. \tag{3.34}$$

This implies that

$$\left(\frac{u_+}{c_+}\right)^{\frac{2m}{m+2}}=\kappa^{-\frac{m}{m+2}}\left(\frac{A_q}{A_+}\right)^m\left(\frac{u_q}{c_q}\right)^{\frac{2m}{m+2}}$$

Hence we have

$$\begin{aligned}\chi'(\kappa;\mathbf{w}_q)&=-\left(\frac{K_{out}}{K_{in}}\right)^{\frac{2}{m+2}}\left(\frac{u_+}{c_+}\right)^{\frac{2m}{m+2}}\kappa^{-\frac{m+4}{m+2}}+\frac{K_{out}}{K_{in}}\left(\frac{A_+}{A_0}\right)^{-m}\kappa^{-2},\\ &=\frac{1}{\kappa^2}\frac{K_{out}}{K_{in}}\left(\frac{A_+}{A_0}\right)^{-m}\left[1-\left(\frac{u_q}{c_q}\right)^{\frac{2m}{m+2}}\left(\frac{A_q}{A_0}\right)^m\left(\frac{K_{in}}{K_{out}}\right)^{\frac{m}{m+2}}\right].\end{aligned} \tag{3.35}$$

This is enough for the proof of the lemma. □

Before investigating the existence of $P^j_{s0s}(\mathbf{w}_q)$, it is necessary to study the behavior of the functions $\varphi(\kappa;\mathbf{w}_q)$ and $\tau(\kappa;\mathbf{w}_q)$. The partial derivative of the function $\varphi(\kappa;\mathbf{w}_q)$ in terms of κ is

$$\frac{\partial\varphi(\kappa;\mathbf{w}_q)}{\partial\kappa}=\left(\frac{u_q}{c_q}\right)^{\frac{2m}{m+2}}\kappa^{-\frac{m}{m+2}}-\left(\frac{A_0}{A_q}\right)^m. \tag{3.36}$$

We denote

$$\kappa^*=\left(\frac{u_q}{c_q}\right)^2\left(\frac{A_q}{A_0}\right)^{m+2}. \tag{3.37}$$

So we have

$$\frac{\partial\varphi(\kappa;\mathbf{w}_q)}{\partial\kappa}\begin{cases}>0, \text{ if } \kappa<\kappa^*,\\ =0, \text{ if } \kappa=\kappa^*,\\ <0, \text{ if } \kappa>\kappa^*.\end{cases} \tag{3.38}$$

Hence we obtain the following lemma.

LEMMA 3.9. *The function* $\varphi(\kappa;\mathbf{w}_q)$ *is increasing when* $\kappa<\kappa^*$ *and decreasing when* $\kappa>\kappa^*$*. It reaches the maximum values at* $\kappa=\kappa^*$*. More precisely the maximum value is given as*

$$\varphi^{\kappa^*}_{max}=\frac{m}{2}\left(\frac{u_q}{c_q}\right)^2\left[\left(\frac{A_q}{A_0}\right)^2-\left(\frac{A_q}{\hat{A}_{j,q}}\right)^2\right]-\left(\frac{\hat{A}_{j,q}}{A_q}\right)^m+\left(\frac{A_0}{A_q}\right)^m. \tag{3.39}$$

In the domain $\kappa\in]0,+\infty[$, the function $\varphi(\kappa;\mathbf{w}_q)$ increases from $\varphi(0;\mathbf{w}_q)$ to the maximum value $\varphi^{\kappa^*}_{max}$, then it decreases from $\varphi^{\kappa^*}_{max}$ to $-\infty$. Moreover we have

$$\varphi(0;\mathbf{w}_q)=-\frac{m}{2}\left(\frac{u_q}{c_q}\right)^2\left(\frac{A_q}{\hat{A}_{j,q}}\right)^2-\left(\frac{\hat{A}_{j,q}}{A_q}\right)^m+\left(\frac{A_0}{A_q}\right)^m. \tag{3.40}$$

We set

$$A^*_{sup} = A_q \left[\frac{m}{2} \left(\frac{u_q}{c_q} \right)^2 \left(\frac{A_q}{\hat{A}_{j,q}} \right)^2 + \left(\frac{\hat{A}_{j,q}}{A_q} \right)^m \right]^{\frac{1}{m}}. \tag{3.41}$$

So if $A_0 > A^*_{sup}$, we have $\varphi(0; \mathbf{w}_q) > 0$. There exists a unique solution denoted as κ^φ_s for the equation $\varphi(\kappa; \mathbf{w}_q) = 0$. Otherwise if $A_0 < A^*_{sup}$, there are two solutions to $\varphi(\kappa; \mathbf{w}_q) = 0$. We use κ^φ_l to denote the one closer to 0, while κ^φ_r is used to denote the remaining one.

REMARK 3.10. *Assume that $u_L > c_L$ and $A^{P_2^l}_{max} \geq A_0 \left[1 - \frac{K_R}{K_L}\right]^{\frac{1}{m}}$, then the inequality holds $\varphi\left(\frac{K_R}{K_L}; \mathbf{w}_L\right) \leq 0$ if one of the following four conditions is satisfied:*

$$\varphi^*_{max} \leq 0; \tag{3.42}$$

$$A_0 > A^*_{sup} \text{ and } \kappa^\varphi_s \leq \frac{K_R}{K_L} < 1; \tag{3.43}$$

$$A_0 \leq A^*_{sup} \text{ and } 1 < \kappa^\varphi_l < \kappa^\varphi_r; \tag{3.44}$$

$$A_0 \leq A^*_{sup} \text{ and } \kappa^\varphi_l < \kappa^\varphi_r \leq \frac{K_R}{K_L} < 1. \tag{3.45}$$

Analogously we can prove the following lemma.

LEMMA 3.11. *The function $\tau(\kappa; \mathbf{w}_q)$ is increasing when $\kappa < \left(\frac{u_q}{c_q}\right)^2 \left(\frac{A_q}{A_0}\right)^{m+2}$ and decreasing when $\kappa > \left(\frac{u_q}{c_q}\right)^2 \left(\frac{A_q}{A_0}\right)^{m+2}$. It reaches the maximum value at $\kappa = \left(\frac{u_q}{c_q}\right)^2 \left(\frac{A_q}{A_0}\right)^{m+2}$ given by*

$$\tau^*_{max} = \frac{m}{2} \left(\frac{u_q}{c_q} \right)^2 \left(\frac{A_q}{A_0} \right)^2 - \frac{m}{2} \left(\frac{u_q}{c_q} \right)^2 - 1 + \left(\frac{A_0}{A_q} \right)^m. \tag{3.46}$$

In addition note that

$$\tau(0; \mathbf{w}_q) = -\frac{m}{2} \left(\frac{u_q}{c_q} \right)^2 - 1 + \left(\frac{A_0}{A_q} \right)^m. \tag{3.47}$$

We define

$$A^*_{s0s} = A_q \left[\frac{m}{2} \left(\frac{u_q}{c_q} \right)^2 + 1 \right]^{\frac{1}{m}}. \tag{3.48}$$

So if $A^*_{s0s} \geq A_0$, the inequality $\tau(0; \mathbf{w}_q) \leq 0$ holds, and vice versa.

REMARK 3.12. *The inequality $\tau(\frac{K_R}{K_L}; \mathbf{w}_q) \leq 0$ holds if one of the following four conditions is satisfied:*

$$\tau^*_{max} \leq 0; \tag{3.49}$$

$$A_0 > A^*_{s0s} \text{ and } \kappa^\tau_s \leq \frac{K_R}{K_L} < 1; \tag{3.50}$$

$$A_0 \leq A^*_{s0s} \text{ and } 1 < \kappa^\tau_l < \kappa^\tau_r; \tag{3.51}$$

$$A_0 \leq A^*_{s0s} \text{ and } \kappa^\tau_l < \kappa^\tau_r \leq \frac{K_R}{K_L} < 1, \tag{3.52}$$

where κ_s^τ, κ_l^τ and κ_r^τ are solutions to $\tau(\kappa;\mathbf{w}_q)=0$.

LEMMA 3.13. *Assume that $u_q^2 > c_q^2$, then the composite wave curve $P_{s0s}^j(\mathbf{w}_q)$ exists when K varies from K_l to K_r, which are defined by*

$$(3.53)\quad]K_l,\ K_r[= \begin{cases}]K_{in},\ K_{out}[, & \text{if } \varphi\left(\frac{K_{out}}{K_{in}};\mathbf{w}_q\right)\le 0,\\ ]\kappa_{s0s}^{\chi,q}K_{in},\ K_{out}[, & \text{if } \varphi\left(\frac{K_{out}}{K_{in}};\mathbf{w}_q\right)>0 \ \&\ \tau\left(\frac{K_{out}}{K_{in}};\mathbf{w}_q\right)\le 0,\\ \emptyset, & \text{otherwise,}\end{cases}$$

where $\kappa_{s0s}^{\chi,q}$ is the solution to $\chi(\kappa;\mathbf{w}_q)=0$.

Proof. It is enough to find the existence region for $P_{s0s}^1(\mathbf{w}_L)$. The other one for $P_{s0s}^2(\mathbf{w}_R)$ can be dealt with in the same manner. According to previous analysis, we only need to identify the existence of $\mathbf{w}_- = J(K;\mathbf{w}_L,K_L)$ and $\mathbf{w} = J(K_R;\mathbf{w}_+,K)$. They are equivalent to finding the region on which $\tau(\kappa;\mathbf{w}_L)\le 0$ and $\chi(\kappa;\mathbf{w}_L)\le 0$ respectively.

If $\varphi\left(\frac{K_R}{K_L};\mathbf{w}_L\right)\le 0$, according to Remark 3.10, one of the four conditions (3.42), (3.43), (3.44), or (3.45) is satisfied. If (3.42) is true, i.e. $\varphi(\kappa;\mathbf{w}_L)<0$ for any $\kappa>0$. Thus from Lemma 3.6, we have $\tau(\kappa;\mathbf{w}_L)<\varphi(\kappa;\mathbf{w}_L)$. So it directly follows that $\tau(\kappa;\mathbf{w}_L)<0$ for $\frac{K_R}{K_L}<\kappa<1$. Likewise we can obtain that $\varphi(\kappa;\mathbf{w}_L)<0$ if one of the remaining conditions (3.43), (3.44) or (3.45) is satisfied. Now we turn to $\chi(\kappa;\mathbf{w}_L)\le 0$ when $\varphi\left(\frac{K_R}{K_L};\mathbf{w}_L\right)\le 0$. Note that

$$(3.54)\qquad \chi\left(\frac{K_R}{K_L}\right)=\tau\left(\frac{K_R}{K_L};\mathbf{w}_L\right) \text{ and } \chi(1;\mathbf{w}_L)=\varphi\left(\frac{K_R}{K_L};\mathbf{w}_L\right).$$

According to Lemma 3.8, if $F_L^{\frac{2m}{m+2}}\left(\frac{A_L}{A_0}\right)^m\left(\frac{K_L}{K_R}\right)^{\frac{m}{m+2}}>1$, we have $\chi'(\kappa)<0$. Hence it holds that

$$\chi(\kappa;\mathbf{w}_L)<\chi\left(\frac{K_R}{K_L}\right)=\tau\left(\frac{K_R}{K_L};\mathbf{w}_L\right)<\varphi\left(\frac{K_R}{K_L};\mathbf{w}_L\right)\le 0.$$

Otherwise if $F_L^{\frac{2m}{m+2}}\left(\frac{A_L}{A_0}\right)^m\left(\frac{K_L}{K_R}\right)^{\frac{m}{m+2}}<1$, we have $\chi'(\kappa;\mathbf{w}_L)>0$. Thus $\chi(\kappa;\mathbf{w}_L)<\chi(1;\mathbf{w}_L)=\varphi\left(\frac{K_R}{K_L};\mathbf{w}_L\right)\le 0$.

If $\varphi\left(\frac{K_{out}}{K_{in}};\mathbf{w}_q\right)>0$ and $\tau\left(\frac{K_{out}}{K_{in}};\mathbf{w}_q\right)\le 0$, with (3.54), we have $\chi\left(\frac{K_R}{K_L}\right)=\tau\left(\frac{K_R}{K_L};\mathbf{w}_L\right)\le 0$ and $\chi(1;\mathbf{w}_L)=\varphi\left(\frac{K_R}{K_L};\mathbf{w}_L\right)>0$. This implies that $\chi'(\kappa;\mathbf{w}_L)>0$ and $F_L^{\frac{2m}{m+2}}\left(\frac{A_L}{A_0}\right)^m\left(\frac{K_L}{K_R}\right)^{\frac{m}{m+2}}<1$. So $\chi\left(\frac{K_R}{K_L};\mathbf{w}_L\right)<\chi(\kappa;\mathbf{w}_L)<\chi(1;\mathbf{w}_L)$. Thus by the intermediate value theorem, there exists a unique solution to $\chi(\kappa;\mathbf{w}_L)=0$ for $\kappa\in]\frac{K_R}{K_L},\ 1[$ denoted by $\kappa_{s0s}^{\chi,l}$.

In the end if $\tau\left(\frac{K_{out}}{K_{in}};\mathbf{w}_q\right)\le 0$, from above we have $\chi(1;\mathbf{w}_L)>0$ and $\chi\left(\frac{K_R}{K_L};\mathbf{w}_L\right)>0$. This leads to the fact that $\chi(\kappa;\mathbf{w}_L)>0$ for any $\kappa\in]\frac{K_R}{K_L},\ 1[$. Thus the stationary wave $\mathbf{w}=\mathbf{J}(K_R;\mathbf{w}_+,K)$ does not exist. This is enough for the proof of the lemma. □

REMARK 3.14. *The equation $\chi(\kappa_{s0s}^{\chi,q};\mathbf{w}_q)=0$ implies that the state $\mathbf{w}_*^c = J(K_{out};\mathbf{w}_+,\kappa_{s0s}^{\chi,q}K_{in})$ is a critical state, where $\mathbf{w}_- = J(\kappa_{s0s}^l K_{in};\mathbf{w}_q,K_{in})$ and $\mathbf{w}_+ = S_1^0(\mathbf{w}_-)$. The subscript $_*$ is used to distinguish this critical state from the one defined in Remark 3.4.*

We consider the monotonic behavior of $P^j_{s0s}(\mathbf{w}_q)$ in terms of the transmural pressure ψ and the velocity u with respect to K. With the help of (2.2), the following relations are satisfied:

$$\left(\frac{\psi_q}{K_{in}}+1\right)^{\frac{1}{m}} u_q = \left(\frac{\psi_-}{K}+1\right)^{\frac{1}{m}} u_-, \tag{3.55}$$

$$\frac{\rho u_q^2}{2}+\psi_q = \frac{\rho u_-^2}{2}+\psi_-, \tag{3.56}$$

$$\left(\frac{\psi_-}{K}+1\right)^{\frac{1}{m}} u_- = \left(\frac{\psi_+}{K}+1\right)^{\frac{1}{m}} u_+, \tag{3.57}$$

$$u_- + \frac{m(\psi_-+K)}{(m+1)\rho u_-} = u_+ + \frac{m(\psi_++K)}{(m+1)\rho u_+}, \tag{3.58}$$

$$\left(\frac{\psi}{K_{out}}+1\right)^{\frac{1}{m}} u = \left(\frac{\psi_+}{K}+1\right)^{\frac{1}{m}} u_+, \tag{3.59}$$

$$\frac{\rho u^2}{2}+\psi = \frac{\rho u_+^2}{2}+\psi_+, \tag{3.60}$$

where $\psi_q=\psi(A_q;K_{in})$, $\psi_-=\psi(A_-;K)$, $\psi_+=\psi(A_+;K)$, $\psi=\psi(A;K_{out})$. From (3.55) and (3.56), we obtain

$$\frac{du_-}{dK} = -\frac{u_-\psi_-}{K\rho(u_-^2-c_-^2)}, \tag{3.61}$$

and

$$\frac{d\psi_-}{dK} = -\rho u_-\frac{du_-}{dK} = \frac{u_-^2\psi_-}{K(u_-^2-c_-^2)}.$$

The relations (3.55) and (3.57) yield

$$\left(\frac{\psi_q}{K_{in}}+1\right)u_q^m = \left(\frac{\psi_-}{K}+1\right)u_-^m. \tag{3.62}$$

Inserting (3.62) into (3.58), we get that

$$u_- + \frac{m(\psi_-+K)}{(m+1)\rho u_-} = u_+ + \frac{mK}{(m+1)\rho}\left(\frac{\psi_q}{K_{in}}+1\right)\frac{u_q^m}{u_+^{m+1}}. \tag{3.63}$$

Taking the derivative of (3.63) in terms of K, after short calculation we have

$$\frac{1}{m+1}\left(1-\frac{c_-^2}{u_-^2}\right)\frac{du_-}{dK}+\frac{m}{(m+1)}\frac{1}{\rho u_-} = \left(1-\frac{c_+^2}{u_+^2}\right)\frac{du_+}{dK}+\frac{c_+^2}{(m+1)Ku_+}. \tag{3.64}$$

Using (3.61) into (3.64), we obtain

$$\frac{du_+}{dK} = \frac{u_+^2\left(\frac{(m+1)-\left(\frac{A_-}{A_0}\right)^m}{\rho u_-}-\frac{c_+^2}{Ku_+}\right)}{(m+1)(u_+^2-c_+^2)}. \tag{3.65}$$

From (3.55), (3.57) and (3.59), we obtain that

$$\left(\frac{\psi_q}{K_{in}}+1\right)u_q^m = \left(\frac{\psi_+}{K}+1\right)u_+^m.$$

This leads to the following relationship with respect to the derivative to K

$$\frac{d\psi_+}{dK} = -\frac{m(\psi_+ + K)}{u_+}\frac{du_+}{dK} + \frac{\psi_+}{K}. \tag{3.66}$$

Moreover we have

$$\left(\frac{\psi_q}{K_{in}} + 1\right) u_q^m = \left(\frac{\psi}{K_{out}} + 1\right) u^m.$$

Thus it follows that

$$\frac{d\psi}{dK} = -\frac{m(\psi + K_R)}{u}\frac{du}{dK}. \tag{3.67}$$

Involving (3.66), (3.67), with (3.60) we have

$$\begin{aligned}
\frac{\rho}{u}(u^2 - c^2)\frac{du}{dK} &= \rho u_+ \frac{du_+}{dK} + \frac{d\psi_+}{dK}, \\
&= \frac{\rho}{u_+}(u_+^2 - c_+^2)\frac{du_+}{dK} + \frac{\psi_+}{K}, \\
&= \frac{u_+}{u_-}\left[1 - \frac{1}{m+1}\left(\frac{A_-}{A_0}\right)^m\right] - \frac{\rho c_+^2}{(m+1)K} + \frac{\psi_+}{K}, \\
&= \frac{u_+}{u_-}\left[1 - \frac{1}{m+1}\left(\frac{A_-}{A_0}\right)^m\right] + \frac{1}{m+1}\left(\frac{A_+}{A_0}\right)^m - 1, \\
&= \frac{A_-}{A_+} - 1 + \frac{1}{m+1}\left(\frac{A_-}{A_0}\right)^m \left(\frac{A_-}{A_+}\right)^2 \left(\left(\frac{A_+}{A_-}\right)^{m+2} - \frac{A_+}{A_-}\right).
\end{aligned} \tag{3.68}$$

Note that

$$\left(\frac{A_+}{A_-}\right)^{m+2} - \left[1 + (m+1)\left(\frac{u_-}{c_-}\right)^2\right]\left(\frac{A_+}{A_-}\right) + (m+1)\left(\frac{u_-}{c_-}\right)^2 = 0.$$

Hence we obtain that

$$\left(\frac{A_+}{A_-}\right)^{m+2} - \frac{A_+}{A_-} = (m+1)\left(\frac{u_-}{c_-}\right)^2\left(\frac{A_+}{A_-} - 1\right). \tag{3.69}$$

Inserting (3.69) into (3.68), we have

$$\begin{aligned}
\frac{\rho}{u}(u^2 - c^2)\frac{du}{dK} &= \frac{A_-}{A_+}\left(1 - \frac{A_-}{A_+}\right)\left(\left(\frac{A_-}{A_0}\right)^m \left(\frac{u_-}{c_-}\right)^2 - \frac{A_+}{A_-}\right), \\
&= \frac{A_-}{A_+}\left(1 - \frac{A_-}{A_+}\right)\left(\frac{\rho u_-^2}{mK} - \frac{A_+}{A_-}\right).
\end{aligned} \tag{3.70}$$

Note that $0 < \frac{A_-}{A_+} < 1$. So the sign of $\frac{\rho}{u}(u^2 - c^2)\frac{du}{dK}$ depends on $\frac{\rho u_-^2}{mK} - \frac{A_+}{A_-}$. In this work for the sake of simplicity we only consider the monotonic curve $P_{s0s}^j(\mathbf{w}_q)$.

ASSUMPTION 3.15. *For any $K \in]K_{in},\ K_{out}[$, we assume the state of $P_{s0s}^j(\mathbf{w}_q)$ satisfies*

$$\frac{\rho u_-^2}{mK} - \frac{A_+}{A_-} > 0 \tag{3.71}$$

or

$$\frac{\rho u_-^2}{mK} - \frac{A_+}{A_-} < 0. \tag{3.72}$$

According to our results in Sections 3.4 and 3.5, this assumption is always satisfied. However if

$$\text{there exists } K \in]K_{in},\ K_{out}[\text{ such that } \frac{\rho u_-^2}{mK} - \frac{A_+}{A_-} = 0, \tag{3.73}$$

the curve $P^j_{s0s}(\mathbf{w}_q)$ does not have the monotonicity property. We cannot exclude this point at the moment. It is left as future work. In addition, due to $u^2 - c^2 < 0$, from (3.70) we obtain

$$\frac{1}{u}\frac{du}{dK} < 0 \text{ if } \quad \frac{\rho u_-^2}{mK} - \frac{A_+}{A_-} > 0, \tag{3.74}$$

and

$$\frac{1}{u}\frac{du}{dK} > 0 \text{ if } \quad \frac{\rho u_-^2}{mK} - \frac{A_+}{A_-} > 0. \tag{3.75}$$

3.3. The classification of L–M and R–M curves for $K_L > K_R$. According to Lemmas 3.2, 3.3, and 3.13, for the supercritical Riemann initial data, we can classify the L–M and R–M curves into three different cases respectively. They are given in Tables 3.1 and 3.2. Each case of the L–M curves will be studied in the following sections. The R–M curve can be treated likewise.

TABLE 3.1
Cases of L–M curves with the supercritical initial data

Case III_l	$A^{P_2^l}_{max} \geq A_0\left[1-\frac{K_R}{K_L}\right]^{\frac{1}{m}};\ u_L > c_L;\ \varphi\left(\frac{K_R}{K_L};\mathbf{w}_L\right) \leq 0$
Case VI_l	$A^{P_2^l}_{max} \geq A_0\left[1-\frac{K_R}{K_L}\right]^{\frac{1}{m}};\ u_L > c_L;\ \varphi\left(\frac{K_R}{K_L};\mathbf{w}_L\right) > 0;\ \tau\left(\frac{K_R}{K_L};\mathbf{w}_L\right) \leq 0$
Case V_l	$A^{P_2^l}_{max} \geq A_0\left[1-\frac{K_R}{K_L}\right]^{\frac{1}{m}};\ u_L > c_L;\ \tau\left(\frac{K_R}{K_L};\mathbf{w}_L\right) > 0$

TABLE 3.2
Cases of R–M curves with the supercritical initial data

Case III_r	$u_R + c_R < 0;\ \varphi\left(\frac{K_L}{K_R};\mathbf{w}_R\right) \leq 0$
Case IV_r	$u_R + c_R < 0;\ \varphi\left(\frac{K_L}{K_R};\mathbf{w}_R\right) > 0;\ \tau\left(\frac{K_L}{K_R};\mathbf{w}_R\right) \leq 0$
Case V_r	$u_R + c_R < 0;\ \tau\left(\frac{K_L}{K_R};\mathbf{w}_R\right) > 0$

3.3.1. Cases of L–M curves. In this section we construct in detail the L–M curves for all possible cases with supercritical initial state. The construction is validated by a series of examples. Unless otherwise stated, the computational region for Riemann problem is $]0,1[$. The equilibrium cross sectional area is $A_0 = 2.1124 \times 10^{-4}\ m^2$. The discontinuity is located at $x = 0.5$.

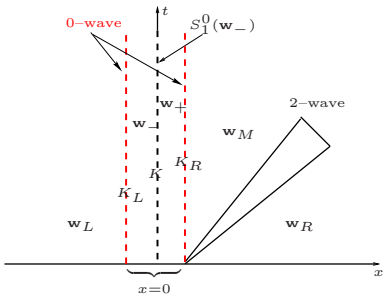

FIG. 3.1. *Wave configuration E*

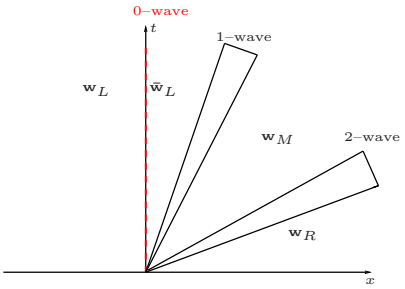

FIG. 3.2. *Wave configuration F*

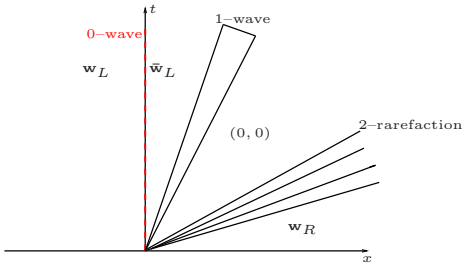

FIG. 3.3. *Wave configuration F_{col}*

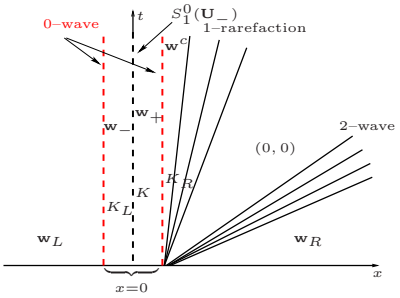

FIG. 3.4. *Wave configuration G_{col}*

3.4. Case III_l: $A_{max}^{P_2^l} \geq A_0 \left[1 - \frac{K_R}{K_L}\right]^{\frac{1}{m}}$; $u_L > c_L$; $\varphi\left(\frac{K_R}{K_L}; \mathbf{w}_L\right) \leq 0$. In this case the possible wave configurations with positive intermediate velocity are the wave configurations A, E, F, and F_{col} see Figures [13, Fig. 3.1], 3.1, 3.2, and 3.3. The wave configuration A has been well studied with examples in [13]. Hence in the present work we just focus on the remaining possible wave configurations E, F and F_{col}. The wave configuration E consists of, from left to right, a resonant wave constituted of three waves: a supersonic stationary wave $\mathbf{w}_- = \mathbf{J}(K; \mathbf{w}_L, K_L)$, a 0–speed 1–shock wave $\mathbf{w}_+ = S_1^0(\mathbf{w}_-)$ and a subcritical stationary wave $\mathbf{w} = \mathbf{J}(K_R; \mathbf{w}_+, K)$, where $K \in]K_R,\ K_L[$. These three waves coalesce on the line $x = 0$. The wave configuration F is classical, which consists of a negative speed 1–shock, followed by a stationary wave located at $x = 0$, and a positive speed 2–wave. The wave configuration F_{col} is associated to the wave configuration F but with a collapsible tube state.

Consequently the corresponding L–M curve $C_L(\mathbf{w}_L)$ consists of the four following parts given by

$$
\begin{aligned}
&P_1^l(\mathbf{w}_L) = \{\mathbf{w} | \mathbf{w} \in T_1(\mathbf{w}_L), u < 0\},\\
&P_2^l(\mathbf{w}_L) = \left\{\mathbf{w} | \mathbf{w} = \mathbf{J}(K_R; \mathbf{w}_-, K_L), \mathbf{w}_- \in T_1(\mathbf{w}_L),\ 0 < u < \bar{\tilde{u}}_{1,L}\right\},\\
&P_3^l(\mathbf{w}_L) = \left\{\mathbf{w} | \mathbf{w} = \mathbf{J}(K_R; \mathbf{w}_+, K);\ \mathbf{w}_+ = S_1^0(\mathbf{w}_-);\ \mathbf{w}_- = \mathbf{J}(K; \mathbf{w}_L, K_L),\ K_R \leq K \leq K_L\right\},\\
&P_4^l(\mathbf{w}_L) = \left\{\mathbf{w} | \mathbf{w} \in T_1(\bar{\mathbf{w}}_L),\ u > \hat{\tilde{u}}_{1,L}\right\},
\end{aligned}
\tag{3.76}
$$

To involve the collapsible tube problem, we define a critical velocity given as

$$
u_{col}^{LM} = \bar{u}_L + \frac{2}{m}\bar{c}_L. \tag{3.77}
$$

So if $u_{col}^{LM} < u_{col}^R$, where u_{col}^R is defined in (3.1), then the Riemann solution has the wave configuration F_{col}. The intermediate state of the wave configuration F_{col}, see Fig.

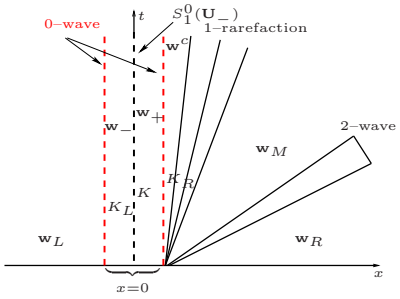

FIG. 3.5. *Wave configuration G*

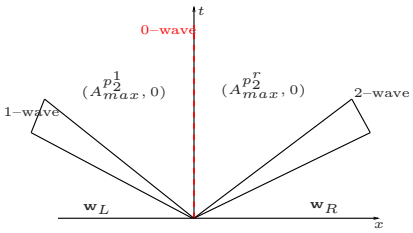

FIG. 3.6. *Wave configuration H*

3.3, is a collapsible state, i.e. with $A = 0$. Otherwise the Riemann solution does not contain the collapsible tube state. More specifically, if the intermediate state $\mathbf{w}_M \in P_2^l(\mathbf{w}_L)$, the exact Riemann solution has the wave configuration A. If the intermediate state $\mathbf{w}_M \in P_3^l(\mathbf{w}_L)$, the exact Riemann solution has the wave configuration E. In addition if the intermediate state $\mathbf{w}_M \in P_4^l(\mathbf{w}_L)$, the exact Riemann solution has the wave configuration F.

The continuity of the L–M wave curve in this case is obvious. From the analysis in Section 3.2, the monotonicity of the L–M curve is determined by the sign of $\frac{\rho u^2}{mK} - \frac{A_+}{A_-}$. According to Assumption 3.15, it is enough to test the sign when $K = K_R$. Specifically it equals to $(\rho\bar{u}_L^2)/(mK_R) - (\hat{\bar{A}}_L)/(\bar{A}_L)$. From (3.74) we have $\frac{du}{dK} < 0$ if $(\rho\bar{u}_L^2)/(mK_R) - (\hat{\bar{A}}_L)/(\bar{A}_L) > 0$; and $\frac{du}{dK} > 0$ if $(\rho\bar{u}_L^2)/(mK_R) - (\hat{\bar{A}}_L)/(\bar{A}_L) < 0$. In addition we have $\frac{d\psi}{dK} = -\frac{1}{K_R u}\frac{du}{dK}$. Thus $\frac{d\psi}{dK} > 0$ if $(\rho\bar{u}_L^2)/(mK_R) - (\hat{\bar{A}}_L)/(\bar{A}_L) > 0$, while $\frac{d\psi}{dK} < 0$ if $(\rho\bar{u}_L^2)/(mK_R) - (\hat{\bar{A}}_L)/(\bar{A}_L) < 0$. Hence u is decreasing while ψ is increasing when K varies from K_R to K_L if $(\rho\bar{u}_L^2)/(mK_R) - (\hat{\bar{A}}_L)/(\bar{A}_L) > 0$ and vice versa.

So on one hand if $(\rho\bar{u}_L^2)/(mK_R) - (\hat{\bar{A}}_L)/(\bar{A}_L) < 0$, we have $\bar{\hat{u}}_L > \hat{\bar{u}}_L$ and $\bar{\hat{\psi}}_L < \hat{\bar{\psi}}_L$. The L–M curve is folding in the $(u,\ \psi)$ plane. A bifurcation appears, see Figure 3.10. This leads to nonunique solutions. For the given initial data, there exists three possible Riemann solutions. On the other hand if $(\rho\bar{u}_L^2)/(mK_R) - (\hat{\bar{A}}_L)/(\bar{A}_L) > 0$, we have $\bar{\hat{u}}_L < \hat{\bar{u}}_L$ and $\bar{\hat{\psi}}_L > \hat{\bar{\psi}}_L$. the L–M curve on $(u,\ \psi)$ space is continuously decreasing. The solution uniquely exist. The examples and details of the unique and nonunique Riemann solutions will be discussed in the following parts.

3.4.1. The unique solution: $(\rho\bar{u}_L^2)/(mK_R) - (\hat{\bar{A}}_L)/(\bar{A}_L) > 0$**.** Three examples have the wave configurations E, F, and F_{col} are used to illustrate our construction respectively. The first example is for the exact solution having the wave configuration E. The initial data and intermediate states are listed in the Table 3.3. Note that $\varphi\left(\frac{K_R}{K_L}; \mathbf{w}_L\right) = -0.368912$ and $\tau\left(\frac{K_R}{K_L}; \mathbf{w}_L\right) = -0.547927$. In addition $(\rho\bar{u}_L^2)/(mK_R) - (\hat{\bar{A}}_L)/(\bar{A}_L) = 4.814028$. The corresponding L–M curve and the exact Riemann solutions are shown in Figure 3.7.

The second example is for a Riemann solution having the wave configuration F. The initial data and states of the exact Riemann solution are listed in Table 3.4. Under this Riemann initial data we have $\varphi\left(\frac{K_R}{K_L}; \mathbf{w}_L\right) = -0.15846$, $\tau\left(\frac{K_R}{K_L}; \mathbf{w}_L\right) = -0.166692$, and $(\rho\bar{u}_L^2)/(mK_R) - (\hat{\bar{A}}_L)/(\bar{A}_L) = 1.928593$. The corresponding L–M

TABLE 3.3
Initial data and intermediate states for an example of Case III_l with the wave configuration E

	$K\ (Pa)$	$A\ (m^2)$	$u\ (m/s)$	S^I
$\mathbf{w}_L$	40000.065331	4.2248×10^{-4}	10.380259	2.0
$\mathbf{w}_-$	29017.111011	4.03365×10^{-4}	10.872157	2.488099
$\mathbf{w}_+$	29017.111011	1.607526×10^{-3}	2.728076	0.441869
$\mathbf{w}_M$	28000.045732	1.700599×10^{-3}	2.578769	0.419263
$\mathbf{w}_R$	28000.045732	1.098391×10^{-3}	0	0

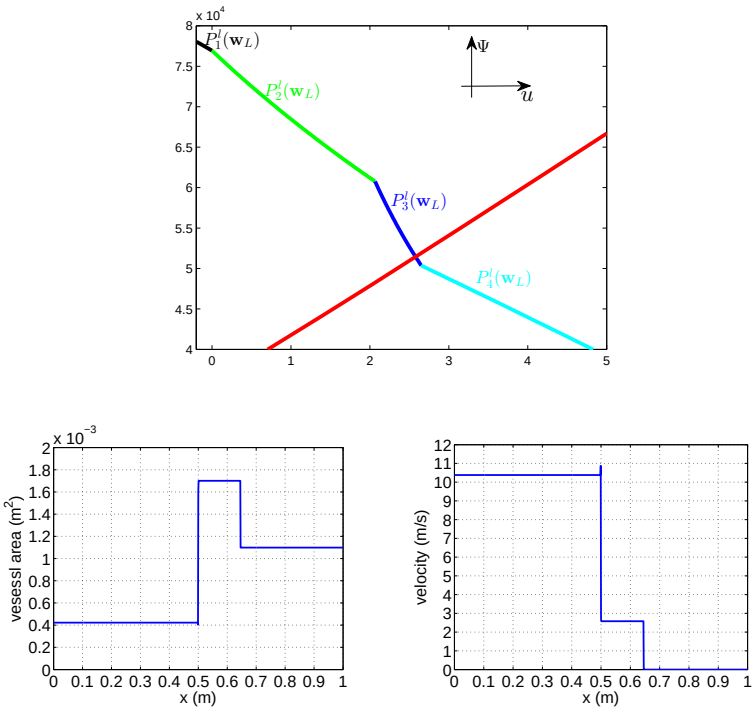

FIG. 3.7. *Top: The L–M curve* $\bigcup_{k=1}^{4} P_k^l(\mathbf{w}_L)$ *to Table 3.3. Bottom: The corresponding vessel area and velocity at* $t = 0.02\ s$.

curve and the exact Riemann solution are shown in Figure 3.8. Clearly we can observe the stationary wave located at $x = 0$, the positive speed 1–shock, and the 2–rarefaction wave.

TABLE 3.4
Initial data and intermediate states for an example of Case III_l with the wave configuration F

	$K\ (Pa)$	$A\ (m^2)$	$u\ (m/s)$	S^I
$\mathbf{w}_L$	0.2	4.2248×10^{-4}	0.015087	1.3
$\bar{\mathbf{w}}_L$	0.14	3.67905×10^{-4}	0.017325	1.847065
$\mathbf{w}_M$	0.14	2.78884×10^{-4}	0.019836	2.266369
$\mathbf{w}_R$	0.14	3.0984×10^{-5}	0	0

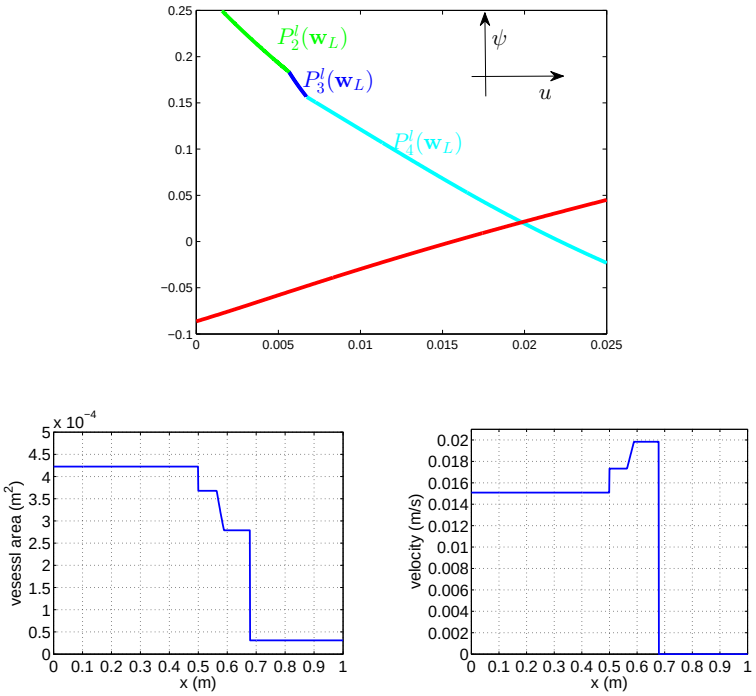

FIG. 3.8. *Top: The L–M curve* $\bigcup_{k=1}^{4} P_k^l(\mathbf{w}_L)$ *to Table 3.4. Bottom: Exact vessel area and velocity at* $t = 8.0$ *s.*

The third example is for the Riemann solution having the wave configuration F_{col}, see Figure 3.3. The initial data and exact Riemann solution are listed in Table 3.5. The equilibrium cross sectional area in this example is $A_0 = 1.0 \times 10^{-4}\ m^2$. The corresponding blood vessel cross sectional area and the velocity are shown in Figure 3.9. We can clearly observe the collapse of the blood vessel in it.

TABLE 3.5
Initial data and intermediate states for an example of Case III_l *with the wave configuration* F_{col}

	$K\ (Pa)$	$A\ (m^2)$	$u\ (m/s)$	S^I
$\mathbf{w}_L$	0.290682	2.0×10^{-4}	0.02098691	1.5
$\bar{\mathbf{w}}_L$	0.203478	1.8140985×10^{-4}	0.0231376	2.025367
$\mathbf{w}_{col}^{LM}$	0.203478	0	0.06883312	–
$\mathbf{w}_{col}^{R}$	0.203478	0	0.938418	–
$\mathbf{w}_R$	0.203478	5.98391×10^{-4}	1.0	64.953862

3.4.2. The nonunique solutions: $(\rho\bar{u}_L^2)/(mK_R) - (\hat{\bar{A}}_L)/(\bar{A}_L) < 0$**.** We define two critical variables $u_1 = u_R + f_R(\hat{\bar{A}}_{1,L}; \mathbf{w}_R)$ and $u_2 = u_R + f_R(\hat{\bar{A}}_{1,L}; \mathbf{w}_R)$. It can be proved that if $u_1 < \hat{\bar{u}}_{1,L}$ and $u_2 > \hat{\bar{u}}_{1,L}$, then there exist three possible solutions with wave configurations A, E and F respectively.

We use an example given in Table 3.6 to illustrate nonunique solutions. The equilibrium cross sectional area is $A_0 = 1.0 \times 10^{-4}\ m^2$. The Riemann initial data

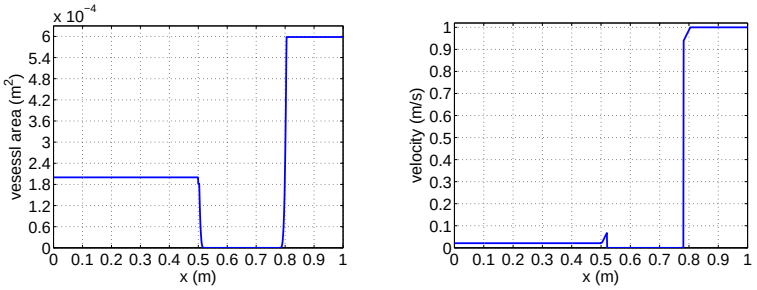

FIG. 3.9. *Exact vessel area and velocity at* $t = 0.3$ *s.*

satisfy $\varphi\left(\frac{K_R}{K_L}; \mathbf{w}_L\right) = -0.405688$, $\tau\left(\frac{K_R}{K_L}; \mathbf{w}_L\right) = -1.19155$, and $(\rho\bar{u}_L^2)/(mK_R) - (\hat{\bar{A}}_L)/(\bar{A}_L) = -5.156529$. The corresponding L–M wave curve is shown on the top of Figure 3.10. The bifurcation can be obviously observed. In addition the states of three possible solutions are shown in Tables 3.7, 3.8, and 3.9. The corresponding solutions are shown in Figure 3.10. Here we use different colors to distinguish the three possible solutions.

TABLE 3.6
Initial data of an example for Case III_l *with three solutions*

	$K\ (Pa)$	$A\ (m^2)$	$u\ (m/s)$	S^I
$\mathbf{w}_L$	58136.483963	1.0×10^{-6}	6.655409	4
$\mathbf{w}_R$	56392.389444	5.038×10^{-6}	0	0

TABLE 3.7
Initial data and intermediate states of an example for Case III_l *with the wave configuration A of Table 3.6*

	$K\ (Pa)$	$A\ (m^2)$	$u\ (m/s)$	S^I
$\mathbf{w}_L$	58136.483963	1.0×10^{-6}	6.655409	4
$\mathbf{w}_-$	58136.483963	8.137909×10^{-6}	0.65858	0.23435
$\mathbf{w}_M$	56392.389444	6.83733×10^{-6}	0.783853	0.291339
$\mathbf{w}_R$	56392.389444	5.038×10^{-6}	0	0

TABLE 3.8
Initial data and intermediate states of an example for Case III_l *with the wave configuration E of Table 3.6*

	$K\ (Pa)$	$A\ (m^2)$	$u\ (m/s)$	S^I
$\mathbf{w}_L$	58136.483963	1.0×10^{-6}	6.655409	4
$\mathbf{w}_-$	57168.798724	1.020605×10^{-6}	6.52104	3.932172
$\mathbf{w}_+$	57168.798724	7.80827×10^{-6}	0.852354	0.309038
$\mathbf{w}_M$	56392.389444	7.199564×10^{-6}	0.924418	0.344383
$\mathbf{w}_R$	56392.389444	5.038×10^{-6}	0	0

TABLE 3.9
Initial data and intermediate states of an example for Case III_l with the wave configuration F of Table 3.6

	$K\ (Pa)$	$A\ (m^2)$	$u\ (m/s)$	S^I
$\mathbf{w}_L$	58136.483963	1.0×10^{-6}	6.655409	4
$\bar{\mathbf{w}}_L$	56392.389444	1.038112×10^{-6}	6.41107	3.875867
$\mathbf{w}_M$	56392.389444	7.493153×10^{-6}	1.035161	0.381805
$\mathbf{w}_R$	56392.389444	5.038×10^{-6}	0	0

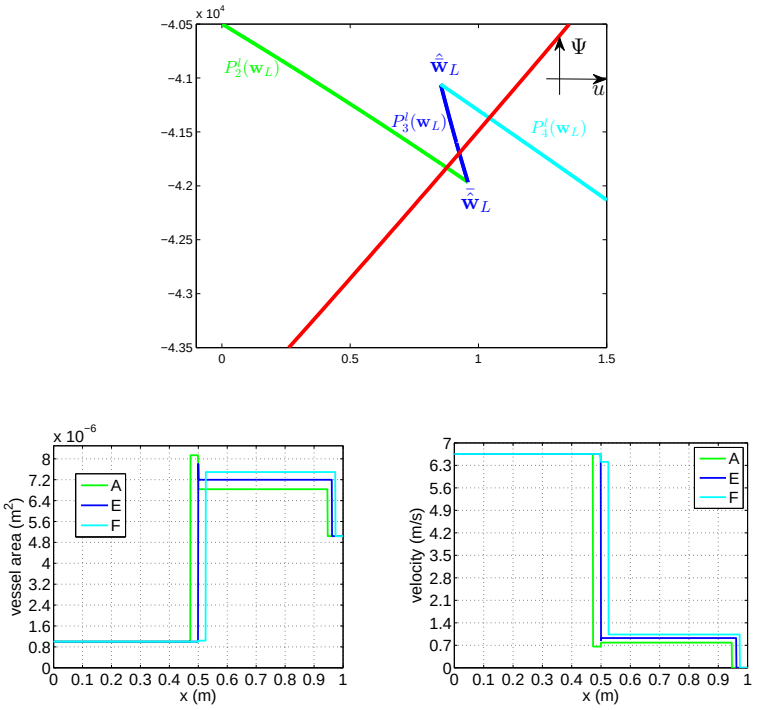

FIG. 3.10. *Top: The L–M curve* $\bigcup_{k=1}^{4} P_k^l(\mathbf{w}_L)$. *Bottom: Exact vessel areas and velocities at* $t = 0.15\ s$.

3.5. Case IV_l: $A_{max}^{P_2^l} \geq A_0 \left[1 - \frac{K_R}{K_L}\right]^{\frac{1}{m}}$, $u_L > c_L$, $\varphi\left(\frac{K_R}{K_L}; \mathbf{w}_L\right) > 0$, and $\tau\left(\frac{K_R}{K_L}; \mathbf{w}_L\right) \leq 0$. In this case the possible wave configurations with positive intermediate velocity are the wave configurations A, B, B_{col}, see Figures in [13, Fig. 3.1, 3.2, 3.5]; and E, F, G, F_{col}, as well as G_{col} in Figures 3.1, 3.2, 3.5, 3.3, and 3.4. The new wave configurations G and G_{col} consist of a resonant wave, which is constituted of a supercritical stationary wave, a zero speed 1–shock, a subcritical stationary wave, and a supercritical 1–rarefaction wave starting from a critical state $\mathbf{w}_*^c$, which is defined in Remark 3.14.

Consequently the L–M curve consists of six segments given by

$$
\begin{aligned}
&P_1^l(\mathbf{w}_L) = \{\mathbf{w}|\mathbf{w} \in T_1(\mathbf{w}_L), u < 0\},\\
&P_2^l(\mathbf{w}_L) = \{\mathbf{w}|\mathbf{w} = \mathbf{J}(K_R; \mathbf{w}_-, K_L), \mathbf{w}_- \in T_1(\mathbf{w}_L),\ 0 < u < u^c\},\\
&P_3^l(\mathbf{w}_L) = \left\{\mathbf{w}|\mathbf{w} = \mathbf{J}(K_R; \mathbf{w}_+, K); \mathbf{w}_+ = S_1^0(\mathbf{w}_-); \mathbf{w}_- = \mathbf{J}(K; \mathbf{w}_L, K_L), K_R \le K \le \kappa_{s0s}^{\chi,l} K_L\right\},\\
&P_4^l(\mathbf{w}_L) = \left\{\mathbf{w}|\mathbf{w} \in T_1(\bar{\mathbf{w}}_L,\ u > \hat{\bar{u}}_{1,L}\right\},\\
&P_5^l(\mathbf{w}_L) = \{\mathbf{w}|\mathbf{w} \in T_1(\mathbf{w}_c), u > u_c\},\\
&P_6^l(\mathbf{w}_L) = \{\mathbf{w}|\mathbf{w} \in T_1(\mathbf{w}_*^c), u > u_*^c\},
\end{aligned}
\tag{3.78}
$$

where $\mathbf{w}^c = (A^c, u^c)^T$, $\kappa_{s0s}^{\chi,l}$, $\mathbf{w}_*^c = (A_*^c, u_*^c)^T$ were defined in Remark 3.4, Lemma 3.13, and Remark 3.14 respectively. Compared with Case III_l, the state $\hat{\bar{\mathbf{w}}}_L$, see Figure 3.10, fails to exist. This is the reason for the appearance of two new branches $P_5^l(\mathbf{w}_L)$ and $P_6^l(\mathbf{w}_L)$, see Figure 3.11. The L–M curve in this case consists of three branches given by $P_1^l(\mathbf{w}_L) \cup P_2^l(\mathbf{w}_L) \cup P_5^l(\mathbf{w}_L)$, $P_3^l(\mathbf{w}_L) \cup P_6^l(\mathbf{w}_L)$ and $P_4^l(\mathbf{w}_L)$.

To involve the collapsible tube states, we define three critical collapsible states: $u_{col,1}^{LM} = \frac{m+2}{m} u^c$, $u_{col,2}^{LM} = \frac{m+2}{m} u_*^c$, and $u_{col,3}^{LM} = \bar{u}_L + \frac{2}{m}\bar{c}_L$. Moreover to precisely determine the wave configuration as in Case IV_l, we introduce three critical states: $u_1 = u_R + f_R(A^c; \mathbf{w}_R)$, $u_2 = u_R + f_R(\hat{\bar{A}}_{1,L}; \mathbf{w}_R)$, and $u_3 = u_R + f_R(A_*^c; \mathbf{w}_R)$. Obviously if $\hat{\bar{u}}_{1,L} > u_2$, there is a unique solution having the wave configuration A. Otherwise there are three possible solutions with different wave configurations located on the corresponding branches of L–M curves, see Figure 3.11.

For the first branch $P_1^l(\mathbf{w}_L) \cup P_2^l(\mathbf{w}_L) \cup P_5^l(\mathbf{w}_L)$, if $u_{col,1}^{LM} < u_{col}^R$ the Riemann solution contains the collapsible tube state and has the wave configuration B_{col}; Otherwise if $u_1 < u^c$, the intermediate state is located on $P_2^l(\mathbf{w}_L)$. The Riemann solution has the wave configuration A; In the end if $u_1 > u^c$ and $u_{col,1}^{LM} > u_{col}^R$, the intermediate state is located on $P_5^l(\mathbf{w}_L)$. The Riemann solution has the wave configuration B.

For the second branch, if $u_{col,2}^{LM} < u_{col}^R$ the Riemann solution contains the collapsible tube state and has the wave configuration G_{col}; otherwise if $u_3 < u_*^c$, the intermediate state is located on $P_3^l(\mathbf{w}_L)$. The Riemann solution has the wave configuration E; On the contrary if $u_3 > u_*^c$ and $u_{col,2}^{LM} > u_{col}^R$, the intermediate state is located on $P_6^l(\mathbf{w}_L)$. The Riemann solution has the wave configuration G.

For the third branch, if $u_{col,3}^{LM} < u_{col}^R$ the Riemann solution contains the collapsible tube state and has the wave configuration F_{col}. Otherwise the intermediate state is located on $P_4^l(\mathbf{w}_L)$. The Riemann solution has the wave configuration F.

Hence there are many possible combinations of the wave configurations, e.g. A, E, F; B, E, F; A, G, F; B, G, F; B_{col}, G, F; and B_{col}, G_{col}, F etc. Here we use four examples to show the nonunique solutions in this case.

3.5.1. Example 1 of Case IV_l. The first example is for nonunique Riemann solutions having the wave configurations B, G, and F. The Riemann initial data and states of exact Riemann solution are shown in Tables 3.10, 3.11, and 3.12 respectively. The L–M curve and three possible solutions are shown in Figure 3.11. The equilibrium cross sectional area for this example is $A_0 = 1.0 \times 10^{-4}\ m^2$. Here we choose the same color for the exact solution as the ones on the corresponding segment of the L–M curve.

3.5.2. Example 2 of Case IV_l. The second example is for nonunique Riemann solutions having the wave configurations A, G, and F. In this example the equilibrium cross sectional area is $A_0 = 1.0 \times 10^{-4}\ m^2$. The Riemann initial data and states of the exact Riemann solution are shown in Tables 3.13, 3.14 and 3.15 respectively. The

TABLE 3.10
Initial data and intermediate states of the nonunique Riemann solutions for an example in Case IV_l with the wave configuration B

	$K\ (Pa)$	$A\ (m^2)$	$u\ (m/s)$	S^I
$\mathbf{w}_L$	0.919219	1.0×10^{-6}	0.023530423	3.556559
$\tilde{\mathbf{w}}_c^{sup}$	0.919219	7.530402×10^{-6}	0.001222575	0.11155
$\mathbf{w}_c$	0.781336	1.390041×10^{-6}	0.006623172	1
$\mathbf{w}_M$	0.781336	3.07432×10^{-7}	0.014947893	3.291043
$\mathbf{w}_R$	0.781336	1.243004×10^{-6}	0.022542384	3.500036

TABLE 3.11
Initial data and intermediate states of the nonunique Riemann solutions for an example in Case IV_l with the wave configuration G

	$K\ (Pa)$	$A\ (m^2)$	$u\ (m/s)$	S^I
$\mathbf{w}_L$	0.919219	1.0×10^{-6}	0.023530423	3.556559
$\mathbf{w}_-$	0.827056	1.206830×10^{-6}	0.019497717	2.964247
$\mathbf{w}_+$	0.827056	6.187583×10^{-6}	0.003802845	0.384212
$\mathbf{w}_c^*$	0.781336	2.944804×10^{-6}	0.007990488	1
$\mathbf{w}_M$	0.781336	6.12679×10^{-6}	0.018366182	3.403310
$\mathbf{w}_R$	0.781336	1.243004×10^{-6}	0.022542384	3.500036

TABLE 3.12
Initial data and intermediate states of the nonunique Riemann solutions for an example in Case IV_l with the wave configuration F

	$K\ (Pa)$	$A\ (m^2)$	$u\ (m/s)$	S^I
$\mathbf{w}_L$	0.919219	1.0×10^{-6}	0.023530423	3.556559
$\bar{\mathbf{w}}_L$	0.781336	1.378420×10^{-6}	0.017070577	2.582817
$\mathbf{w}_M$	0.781336	8.40823×10^{-7}	0.020143824	3.448709
$\mathbf{w}_R$	0.781336	1.243004×10^{-6}	0.022542384	3.500036

L–M curve and three possible solutions are shown in Figure 3.12. We also choose the colors to match the ones on the L–M curve. Note that in Figure 3.11, the right cross sectional area A_R takes a larger value compared with the first example.

TABLE 3.13
Initial data and intermediate states of the nonunique Riemann solutions for an example in Case IV_l with the wave configuration A

	$K\ (Pa)$	$A\ (m^2)$	$u\ (m/s)$	S^I
$\mathbf{w}_L$	0.919219	1.0×10^{-6}	0.023530423	3.556559
$\mathbf{w}_-$	0.919219	7.533525×10^{-6}	0.001214575	0.110809
$\mathbf{w}_M$	0.781336	1.493519×10^{-6}	0.006126494	0.837644
$\mathbf{w}_R$	0.781336	1.0×10^{-5}	0.0225423840	2.078216

3.5.3. Example 3 of Case IV_l. The third example is for the solutions having the wave configurations A, E, and F. In this example the equilibrium cross sectional area is $A_0 = 0.01m^2$. The Riemann initial data and states of exact Riemann solution are shown in Tables 3.16, 3.17, and 3.18 respectively. The L–M curve and three

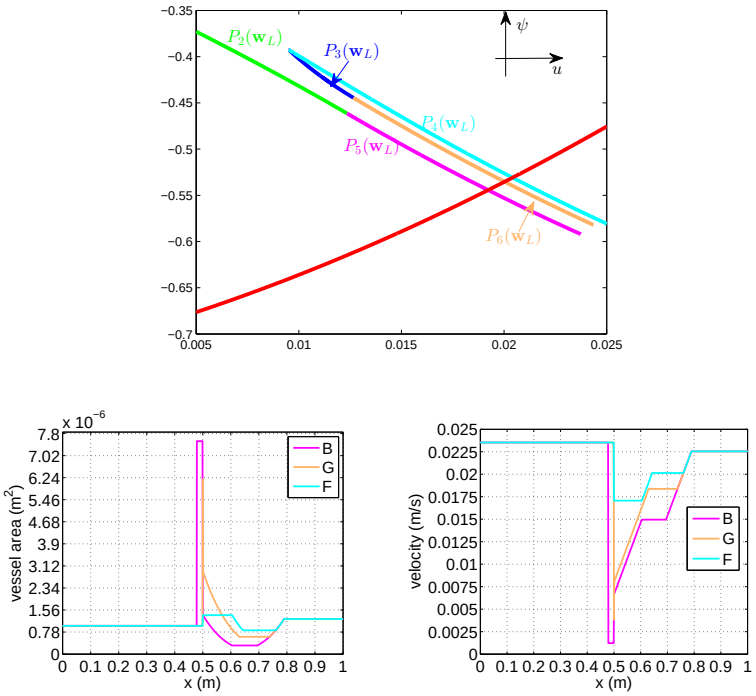

FIG. 3.11. *Top: The L–M curve* $\bigcup_{k=1}^{6} P_k^l(\mathbf{w}_L)$ *of Tables 3.10, 3.11 and 3.12. Bottom: The corresponding exact vessel area and velocity at* $t = 10.0$ *s.*

TABLE 3.14

Initial data and intermediate states of the nonunique Riemann solutions for an example in Case IV$_l$ with the wave configuration G

	K (Pa)	A (m^2)	u (m/s)	S^I
$\mathbf{w}_L$	0.919219	1.0×10^{-6}	0.023530423	3.556559
$\mathbf{w}_-$	0.827056	1.206830×10^{-6}	0.019497717	2.964247
$\mathbf{w}_+$	0.827056	6.187583×10^{-6}	0.003802845	0.384212
$\mathbf{w}_c^*$	0.781336	2.944804×10^{-6}	0.007990488	1
$\mathbf{w}_M$	0.781336	2.409688×10^{-6}	0.009553434	1.257072
$\mathbf{w}_R$	0.781336	1.0×10^{-5}	0.022542384	2.078216

TABLE 3.15

Initial data and intermediate states of the nonunique Riemann solutions for an example in Case IV$_l$ with the wave configuration F

	K (Pa)	A (m^2)	u (m/s)	S^I
$\mathbf{w}_L$	0.919219	1.0×10^{-6}	0.023530423	3.556559
$\bar{\mathbf{w}}_L$	0.781336	1.378420×10^{-6}	0.017070577	2.582817
$\mathbf{w}_M$	0.781336	2.983457×10^{-7}	0.011220750	1.399693
$\mathbf{w}_R$	0.781336	1.0×10^{-5}	0.022542384	2.078216

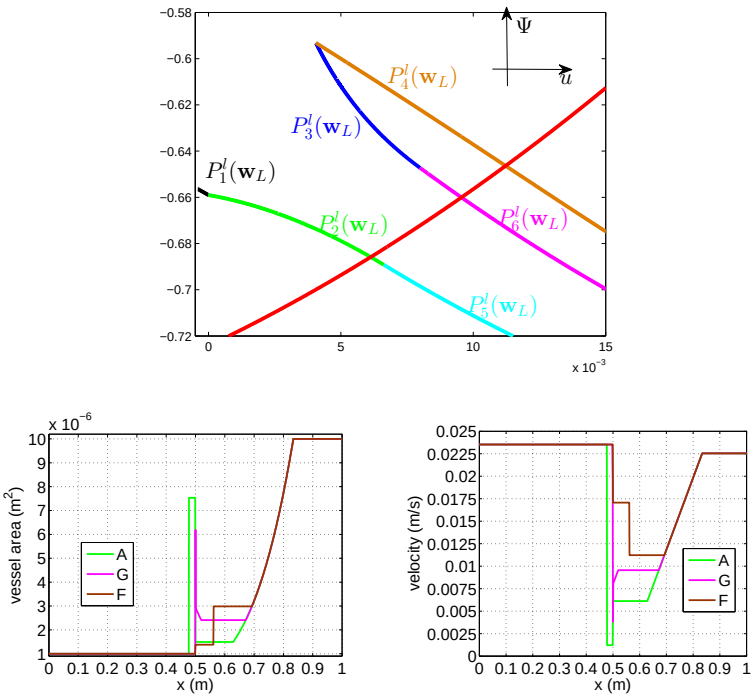

FIG. 3.12. *Top: The L–M curve* $\bigcup_{k=1}^{6} P_k^l(\mathbf{w}_L)$ *of Tables 3.13, 3.14 and 3.15. Bottom: The corresponding exact vessel area and velocity at* $t = 10.0$ *s.*

possible solutions are shown in Figure 3.13.

TABLE 3.16
Initial data and intermediate states of the nonunique Riemann solutions for an example in Case IV_l *with the wave configuration A*

	$K\ (Pa)$	$A\ (m^2)$	$u\ (m/s)$	S^l
$\mathbf{w}_L$	5813.648396	1.0×10^{-4}	1.315390626	2.5
$\mathbf{w}_-$	5813.648396	$4.11231591 \times 10^{-4}$	0.302890497	0.404249
$\mathbf{w}_M$	5581.102460	$2.15004128 \times 10^{-4}$	0.579329067	0.909283
$\mathbf{w}_R$	5581.102460	8.0383910×10^{-5}	0	0

TABLE 3.17
Initial data and intermediate states of the nonunique Riemann solutions for an example in Case IV_l *with the wave configuration E*

	$K\ (Pa)$	$A\ (m^2)$	$u\ (m/s)$	S^l
$\mathbf{w}_L$	5813.648396	1.0×10^{-4}	1.315390626	2.5
$\mathbf{w}_-$	5770.653747	$1.02649664 \times 10^{-4}$	1.281436853	2.428594
$\mathbf{w}_+$	5770.653747	$3.94978467 \times 10^{-4}$	0.333028440	0.450646
$\mathbf{w}_M$	5581.102460	$2.20254785 \times 10^{-6}$	0.597213190	0.950928
$\mathbf{w}_R$	5581.102460	8.0383910×10^{-5}	0	0

TABLE 3.18
Initial data and intermediate states of the nonunique Riemann solutions for an example in Case IV_l with the wave configuration F

	$K\ (Pa)$	$A\ (m^2)$	$u\ (m/s)$	S^I
$\mathbf{w}_L$	5813.648396	1.0×10^{-4}	1.315390626	2.5
$\bar{\mathbf{w}}_L$	5581.102460	$1.18171008 \times 10^{-4}$	1.113124656	2.070931
$\mathbf{w}_M$	5581.102460	$2.43225666 \times 10^{-4}$	0.673363464	1.045916
$\mathbf{w}_R$	5581.102460	8.0383910×10^{-5}	0	0

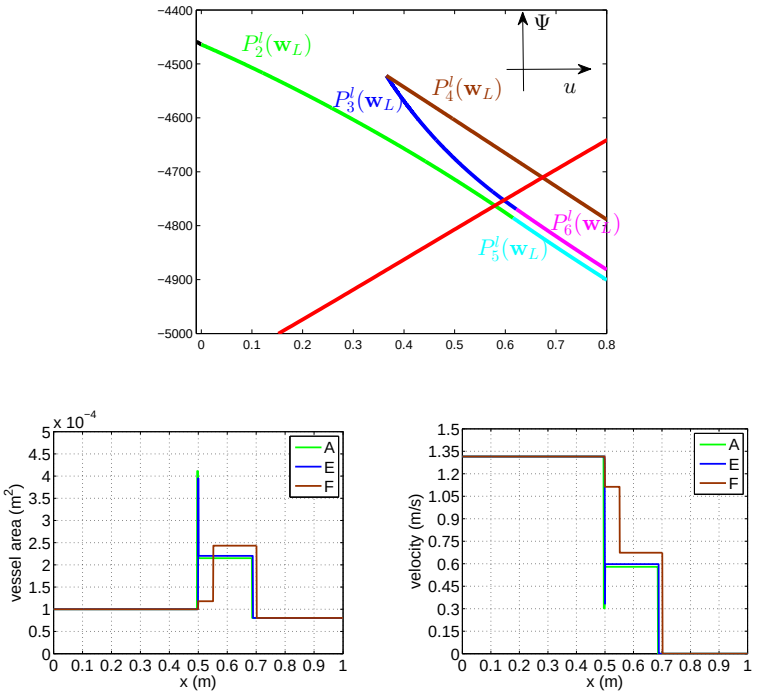

FIG. 3.13. *Top: The L–M curve* $\bigcup_{k=1}^{6} P_k^l(\mathbf{w}_L)$ *of Tables 3.16, 3.17 and 3.18. Bottom: The corresponding exact vessel area and velocity at* $t = 0.2$ *s.*

3.5.4. Example 4 of Case IV_l. The last example is for the solutions having the wave configurations B_{col}, G_{col}, and F. The Riemann initial data and states of exact Riemann solution are shown in Tables 3.19, 3.20 and 3.21 respectively. The L–M curve and three possible solutions are shown in Figure 3.11. The equilibrium cross sectional area in this example is $A_0 = 1.0 \times 10^{-4}\ m^2$.

3.6. Case V_l: $A_{max}^{P_2^l} \geq A_0 \left[1 - \frac{K_R}{K_L}\right]^{\frac{1}{m}}$, $u_L > c_L$, and $\varphi\left(\frac{K_R}{K_L}; \mathbf{w}_L\right) > 0$. With the help of $\varphi\left(\frac{K_R}{K_L}; \mathbf{w}_L\right) > 0$, two branches $P_3^l(\mathbf{w}_L) \cup P_6^l(\mathbf{w}_L)$ and $P_4^l(\mathbf{w}_L)$ of the L–M curve in Case IV_l entirely disappear. Hence the Riemann solution in this case can only have the wave configurations A and B, see [13, Fig. 3.1, 3.2]. Consequently the

TABLE 3.19
Initial data and intermediate states of the nonunique Riemann solutions for an example in Case IV_l with the wave configuration B_{col}

	$K\ (Pa)$	$A\ (m^2)$	$u\ (m/s)$	S^I
$\mathbf{w}_L$	0.290682	1.0×10^{-5}	0.01323213	2.0
$\tilde{\mathbf{w}}_c^{sup}$	0.290682	3.1389752×10^{-5}	0.003708	0.127727
$\mathbf{w}_c$	0.24708	1.6769675×10^{-5}	6.941293×10^{-3}	1
$\mathbf{w}_{col,1}^{LM}$	0.24708	0	0.039696	$--$
$\mathbf{w}_{col}^{R}$	0.24708	0	0.035755	$--$
$\mathbf{w}_R$	0.24708	1.243004×10^{-6}	0.050242	13.872122

TABLE 3.20
Initial data and intermediate states of the nonunique Riemann solutions for Case IV_l with the wave configuration G_{col}

	$K\ (Pa)$	$A\ (m^2)$	$u\ (m/s)$	S^I
$\mathbf{w}_L$	0.290682	1.0×10^{-5}	0.01323213	2.0
$\mathbf{w}_-$	0.263707	1.176424×10^{-5}	0.011247756	1.713854
$\mathbf{w}_+$	0.263707	2.7075627×10^{-5}	0.0048871	0.604582
$\mathbf{w}_c^*$	0.24708	1.8580458×10^{-5}	0.00712153	1
$\mathbf{w}_{col,2}^{LM}$	0.24708	0	0.035608	–
$\mathbf{w}_{col}^{R}$	0.24708	0	0.035755	–
$\mathbf{w}_R$	0.24708	1.243004×10^{-6}	0.050242	13.872122

TABLE 3.21
Initial data and intermediate states of the nonunique Riemann solutions for Case IV_l with the wave configuration F

	$K\ (Pa)$	$A\ (m^2)$	$u\ (m/s)$	S^I
$\mathbf{w}_L$	0.290682	1.0×10^{-5}	0.01323213	2.0
$\bar{\mathbf{w}}_L$	0.24708	1.3749732×10^{-5}	0.009623554	1.456977
$\mathbf{w}_M$	0.24708	1.231459×10^{-14}	0.035899623	993.517825
$\mathbf{w}_R$	0.24708	1.243004×10^{-6}	0.050242	13.872122

L–M curve are defined by

$$
\begin{aligned}
&P_1^l(\mathbf{w}_L) = \{\mathbf{w} | \mathbf{w} \in T_1(\mathbf{w}_L), u < 0\}, \\
&P_2^l(\mathbf{w}_L) = \{\mathbf{w} | \mathbf{w} = \mathbf{J}(K_R; \mathbf{w}_-, K_L), \mathbf{w}_- \in T_1(\mathbf{w}_L),\ 0 < u < u^c\}. \\
&P_3^l(\mathbf{w}_L) = \{\mathbf{w} | \mathbf{w} \in T_1(\mathbf{w}^c), u > u^c\},
\end{aligned} \tag{3.79}
$$

Note that the L–M curve in this case is continuously decreasing. Therefore the Riemann solution in this case uniquely exists. We use one example given in Table 3.22 to demonstrate the Riemann solution for the wave configuration B. The result is shown in Figure 3.15, where $A_0 = 0.01\ m^2$.

3.7. Cases of R–M curves. According to Table 3.2, the R–M curves contain three different cases. The cases of the R–M curves can be treated likewise as the ones of the L–M curves. The corresponding wave configurations with negative intermediate velocity can be denoted by E^T, F^T, G^T, F_{col}^T, and G_{col}^T to denote the appropriate symmetric cases of the ones with the positive intermediate velocity. The segments of R–M curve will also be denoted as $P_j^r(\mathbf{w}_R)$, $j = 1, \cdots, 6$. The segment $P_1^r(\mathbf{w}_R)$ defined

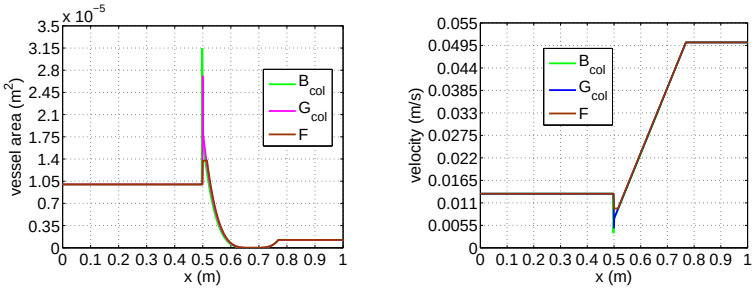

FIG. 3.14. *The corresponding exact vessel area and velocity at $t = 5.0\ s$.*

TABLE 3.22
Initial data and intermediate states of an example for Case V_l with the wave configuration B.

	$K\ (Pa)$	$A\ (m^2)$	$u\ (m/s)$	S^I
$\mathbf{w}_L$	5813.648396	1.0×10^{-4}	1.315391	2.5
$\tilde{\mathbf{w}}_c^{sup}$	5813.648396	4.847543×10^{-4}	0.125030	0.160148
$\mathbf{w}_c$	5232.283557	1.167995×10^{-4}	0.518915	1
$\mathbf{w}_M$	5232.283557	6.44362×10^{-5}	0.805707	1.8016
$\mathbf{w}_R$	5232.283557	1.03839×10^{-5}	0	0

in [13, p. 10,(3.6)] is common for all cases. The segment $P_2^r(\mathbf{w}_R) = P_{ES}^2(\mathbf{w}_R)$ has been well studied in Lemma 3.3 and Remark 3.5. The segment $P_3^r(\mathbf{w}_R) = P_{s0s}^2(\mathbf{w}_R)$ for Cases III_r and IV_r has been established in Lemma 3.53. Moreover, we outline the additional segments in the following.

In Case III_r, the R–M curve consists of four segments. The remaining segment is $P_4^r(\mathbf{w}_R) = T_2(\bar{\mathbf{w}}_R)$. The nonunique solutions having the wave configurations A^T, E^T, and F^T might occur for some given initial data if they satisfy $(\rho\bar{u}_R^2)/(mK_L) - \hat{(\bar{A}_{2,R})}/(\bar{A}_R) < 0$. Otherwise the solution is unique with one of the wave configurations A^T, E^T, F^T, or F_{col}^T. The solution with the wave configuration F_{col}^T contains collapsible states and is identified by $u_{col}^{RM} > u_{col}^L$, where

$$u_{col}^{RM} = \bar{u}_R - \frac{2}{m}\bar{c}_R. \tag{3.80}$$

In Case IV_r, the R–M curve consists of six segments. The remaining segments are $P_4^r(\mathbf{w}_R) = T_2(\bar{\mathbf{w}}_R)$, $P_5^r(\mathbf{w}_R) = T_2(\mathbf{w}^c)$, and $P_6^r(\mathbf{w}_R) = T_2(\mathbf{w}_*^c)$, where the critical state $\mathbf{w}^c = J(K_L; \tilde{\mathbf{w}}_{l,sup}^c, K_R)$, $\tilde{\mathbf{w}}_{l,sup}^c$ and $\mathbf{w}^c$ were defined in Remark 3.4; The critical state $\mathbf{w}_*^c$ was derived in (3.14). Analogously to Case IV_l, these six segments of the R–M curve form three different branches: $P_1^r(\mathbf{w}_R) \cup P_2^r(\mathbf{w}_R) \cup P_5^r(\mathbf{w}_R)$, $P_3^r(\mathbf{w}_R) \cup P_6^r(\mathbf{w}_R)$ and $P_4^r(\mathbf{w}_R)$. This leads to multiple solutions for the given initial data. The possible wave configurations with negative intermediate velocity are the wave configurations A^T, B^T, E^T, F^T, G^T, B_{col}^T, F_{col}^T, and G_{col}^T. The wave configurations A^T, B^T, and B_{col}^T are associated to the first branch. The wave configuration E^T, G^T, and G_{col}^T are on the second branch. While the wave configuration F^T and F_{col}^T are on the third branch. Since each branch can be proved to be continuously monotonic, the Riemann solutions are the combination of the wave configurations on three branches if nonunique Riemann solutions exist.

In Case V_r, the R–M curve consists of two segments. The segment $P_3^r(\mathbf{w}_R) = T_2(\mathbf{w}^c)$. As in Case IV_r, the critical state $\mathbf{w}^c = J(K_L; \tilde{\mathbf{w}}_{l,sup}^c, K_R)$. The states $\tilde{\mathbf{w}}_{l,sup}^c$

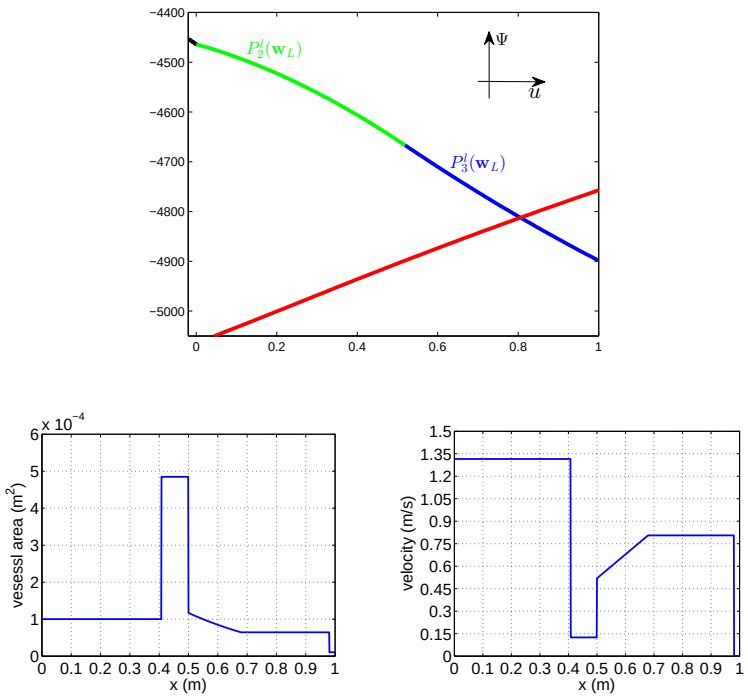

FIG. 3.15. *Top: The L–M curve* $\bigcup_{k=1}^{3} P_k^l(\mathbf{w}_L)$ *for Table 3.22. Bottom: Exact vessel area and velocity at* $t = 0.5$ *s.*

and $\mathbf{w}^c$ are defined in Remark 3.4; The critical state $\mathbf{w}_*^c$ was derived in (3.14). The R–M curve in this case is is continuously decreasing, i.e. the Riemann solution in this case uniquely exists.

For the given Riemann initial data, we define the L–M and R–M curves with the supercritical data according to the previous sections. The L–M and R–M curves with the subcritical data has been defined in [13, Sec. 3.3, 3.4]. Based on them, the exact Riemann solutions can be uniformly solved by the algorithm in [13, Sec. 3.5].

4. Conclusions. In this paper, uniform framework, we have completely solved the Riemann problem for a 3×3 resonant system of equations governing the flow in a collapsible tube with discontinuous material properties. Here we have focused on the case of supercritical Riemann initial data, while in the companion paper [13] we focused on the subcritical case. The non-unique Riemann solutions appear for certain supercritical initial data due to the bifurcation of the L–M and R–M curves. Several examples are given for positive intermediate velocity. The Riemann solutions obtained reveal the mathematical structure of the model and they can also be directly used to assess the performance of numerical methods intended for solving more realistic problems.

REFERENCES

[1] J. Alastruey, W. Khir, K.S. Matthys, P. Segers, S.J. SherwinK, P.R. Verdonck, K.H. Parker, and J. Peiró",*Pulse wave propagation in a model human arterial network: Assessment of 1-D visco-elastic simulations against in vitro measurements.* J. Biomech., 44(2011), pp. 2250-2258.

[2] N. Andrianov and G. Warnecke,*On the solution to Riemann problem for compressible duct flow,* SIAM J. Appl. Math., 64(2004), pp. 878-901.

[3] N. Andrianov and G. Warnecke,*The Riemann problem for Baer-Nunziato model of two phase flows,* J. Comput. Phys., 195(2004) pp. 434-464.

[4] B. S. Brook, S. A. E. G: Falle, and T. J. Pedley, *Numerical solutions for unsteady gravity–driven flows in collapsible tubes: evolution and roll–wave instability of steady state*, J. Fluid Mech., 396(1999), pp. 223-256.

[5] C. G. Caro, T. J. Pedley, R. C. Schroter, and W. A. Seed, The mechanics of the circulation, Second Edition, Cambridge, 2012.

[6] S. Čanić, C.J. Hartley, D. Rosenstrauch, J. Tambača, G. Guidoboni, and A. Mikelić, *Blood flow in compliant arteries: an effective viscoelastic reduced model, numerical, and experimental validation*, Ann. Biomed. Eng., 34(2006), pp. 575-592.

[7] W. Dahmen, S. Müller, and A. Voss, *Riemann problem for the Euler equations with nonconvex equation of state including phase transitions,* Analysis and Numerics for Conservation Laws, Springer, Berlin, (2005), pp. 137-162.

[8] G. Dalmaso, P.L. LeFloch and F. Murat, *Definition and weak stability of non-conservative products*, J. Math. Pures. Appl., 74(1995), pp. 483-548.

[9] D. Elad, R.D. Kamm, and A.H. Shapiro, *Mathematical simulation of forced expiration*, J. Appl. Physiol., 65(1988), pp. 14-25.

[10] L. Formaggia, A. Quarteroni and A. Veneziani, Cardiovascular Mathematics, Modelling, simulation and application series. Springer-Verlag, Berlin, Heidelberg, New York, 2009.

[11] E. Han and G. Warnecke, *Exact Riemann solutions to shallow water equations*, Q. Appl. MATH. , accept, 2012.

[12] E. Han and M. Hantke and G. Warnecke, *Exact Riemann solutions in ducts with discontinuous cross-section*, J. Hyp. Diff. Equations, 9(2012), 403-449.

[13] E. Han, G. Warnecke, E. F. Toro and A Siviglia, *On Riemann solutions to weakly hyperbolic systems: Part 1. Modelling subcritical flows in arteries*, to be appeared .

[14] J. M. Hong, *An extension of Glimms method to inhomogeneous strictly hyperbolic systems of conservation laws by weaker than weak solutions of the Riemann problem*, J. Differential Equations, 222(2006), pp. 515-549.

[15] J. Hong and B. Temple, *The Generic Solution of the Riemann Problem in a Neighborhood of a Point of Resonance for Systems of Nonlinear Balance Laws,* Methods Appl. Anal., 10(2003), pp. 279-294.

[16] E. Isaacson and B. Temple, *Nonlinear resonance in systems of conservation-laws*, SIAM J Appl. Math. 52(1992), pp. 1260-1278.

[17] R.D. Kamm and A.H. Shapiro , *Unsteady flow in a collapsible tube subjected to external pressure or body forces,* J. Fluid Mech., 95(1979), pp. 1-78.

[18] D.N. Ku,*Blood flow in arteries,* Annu. Rev. Fluid Mech., 129(1997), pp. 399-434.

[19] D.N. Ku, M.N. Zeigler, and J.M. Downing , *One-dimensional steady inviscid flow through a stenotic collapsible tube,* J. Biomech. Eng-T. ASME, 112(1990), pp. 444-450.

[20] P. G. Lefloch and M. D. Thanh, *The Riemann problem for fluid flows in a nozzle with discontinuous cross–section,* Commun. Maths. Sci., 1(2003), 763-797.

[21] P. G. LeFloch and M. D. Thanh, *The Riemann problem for shallow water equations with discontinuous Topography,* Commun. Maths. Sci., 5(2007), pp. 865-885.

[22] P. G. LeFloch and M. D. Thanh, *A Godunov-type method for the shallow water equations with discontinuous topography in the resonant regime,* J. Comput. Physics, 230(2011), pp. 7631-7660.

[23] R.J. LeVeque, Finite Volume Methods for Hyperbolic Problems, Cambridge University Press, 2002.

[24] F.Y. Liang, S. Takagi, R. Himeno, and H. Liu, *Biomechanical characterization of ventricular-arterial coupling during aging: a multi-scale model study,* J. Biomech., 42(2009) pp. 692-704.

[25] T. P. Liu, *Transonic gas flow in a duct of varying area.* Arch. Rat. Mech. Anal., 23(1982) pp. 1-18.

[26] T. P. Liu, *Nonlinear resonance for quasilinear hyperbolic equation,* J. Math. Phys., 28(1987) pp. 2593-2602.

[27] D. Marchesin and P. J. Paes-Leme, *A Riemann problem in gas dynamics with bifurcation,* Comp. Maths. Appls., 12(1986), pp. 433-455.

[28] M.S. Olufsen, C.S. Peskin, W.Y. Kim, E.M. Pedersen, A. Nadim and J. Larsen, *Numerical simulation and experimental validation of blood flow in arteries with structured-tree outflow conditions.* Annals. Biomed. Engng., **28** (2000), pp. 1281–1299.

[29] T J. Pedley, The fluid dynamics of large blood vessels, Cambridge University Press, 1980.

[30] A. Quarteroni, M. Tuveri and A. Veneziani, *Computational vascular fluid dynamics: problems, models and methods,* Comp. Visual. Science, 2(2000), pp.63-197.

[31] A. Siviglia and M. Toffolon, *Steady analysis of transcritical flows in collapsible tubes with discontinuous mechanical properties: implications for arteries and veins,* J Fluid Mech., 7362013, pp. 195-215.

[32] M.D. Thanh, *The Riemann problem for a non-isentropic fluid in a nozzle with discontinuous cross-sectional area*, SIAM J. Appl. Math. , 69 (2009), pp. 1501-1519.

[33] E. F. Toro, Riemann solvers and numerical methods for fluid dynamics(3rd edition), Springer-Verlag, 2009

[34] E. F. Toro and A Siviglia, *Simplified blood flow model with discontinuous vessel properties: analysis and exact solutions. Modelling Physiological Flows Series: Modelling, Simulation and Applications. Editors: D. Ambrosi, A. Quarteroni and G. Rozza. Springer-Verlag,* 2011

[35] E. F. Toro and A Siviglia, *Flow in collapsible tubes with discontinuous mechanical properties: mathematical model and exact solutions. Commun. Comput. Phys.*, 13(2013), pp. 361-385.